



# 1 Selecting CMIP6 GCMs for CORDEX Dynamical 2 Downscaling over Southeast Asia Using a Standardised 3 Benchmarking Framework

4 Phuong Loan Nguyen<sup>1,2</sup>, Lisa V. Alexander<sup>1,2</sup>, Marcus J. Thatcher<sup>3</sup>, Son C. H. Truong<sup>3</sup>,  
5 Rachael N. Ispording<sup>1,2</sup>, John L. McGregor<sup>3</sup>

6 <sup>1</sup>ARC Centre of Excellence of Climate Extremes and Climate Change Research Centre, UNSW Sydney, Sydney,  
7 NSW 2052, Australia

8 <sup>2</sup>ARC Centre of Excellence for the Weather of the 21<sup>st</sup> Century, UNSW Sydney, Sydney, NSW 2052, Australia

9 <sup>3</sup>CSIRO Environment, Commonwealth Scientific and Industrial Research Organisation, Aspendale, Victoria

10 *Correspondence to:* Phuong Loan Nguyen ([phuongloan.nguyen@unsw.edu.au](mailto:phuongloan.nguyen@unsw.edu.au))

11 **Abstract.** Downscaling global climate models (GCMs) provides crucial, high-resolution data needed for informed  
12 decision-making at regional scales. However, there is no uniform approach to select the most suitable GCMs.  
13 Over Southeast Asia (SEA), observations are sparse and have large uncertainties, complicating GCM selection  
14 especially for rainfall. To guide this selection, we apply a standardised benchmarking framework to select CMIP6  
15 GCMs for dynamical downscaling over SEA, addressing current observational limitations. This framework  
16 identifies fit-for-purpose models through a two-step process: (a) selecting models that meet minimum  
17 performance requirements in simulating the fundamental characteristics of rainfall (e.g., bias, spatial pattern,  
18 annual cycle, and trend) and (b) selecting models from (a) to further assess whether key precipitation drivers  
19 (monsoon) and teleconnections from modes of variability are captured [El Niño-Southern-Oscillation (ENSO)  
20 and Indian Ocean Dipole (IOD)]. GCMs generally exhibit wet biases, particularly over the complex terrain of the  
21 Maritime Continent. Evaluations from the first step identify 19 out of 32 GCMs that meet our minimum  
22 performance expectations in simulating rainfall. These models also consistently capture atmospheric circulations  
23 and teleconnections with modes of variability over the region but overestimate their strength. Ultimately, we  
24 identify eight GCMs meeting our performance expectations. There are obvious, high-performing GCMs from  
25 allied modelling groups, highlighting the dependency of the subset of models identified from the framework.  
26 Therefore, further tests on model independence, data availability, and future climate change spread are conducted,  
27 resulting in a final sub-set of two independent models that align with our a priori expectations for downscaling  
28 over CORDEX-SEA.

29 **Keywords:** CORDEX, regional climate models, CMIP6, standardised benchmarking framework, GCM selection.



## 30 **1 Introduction**

31 The Sixth Assessment Report (AR6) of the Intergovernmental Panel on Climate Change (IPCC) underscores, with  
32 high confidence, the escalating water-related risks, losses and damages associated with each increment of global  
33 warming (Ipcc, 2023). The report specifically notes a projected increase in the frequency and intensity of heavy  
34 rainfall, leading to an increased risk of rain-generated localised flooding, particularly over coastal and low-lying  
35 cities and regions [Section 3 (Ipcc, 2023)]. Therefore, climate projections at regional scales are required to inform  
36 climate change adaptation strategies and enhance resilience efforts.

37 Different types of models have been developed and have become fundamental tools for assessing future regional  
38 climate changes, including state-of-the-art Global Climate Models (GCMs) and Regional Climate Models  
39 (RCMs). GCMs are generally used to explore climate interactions and underpin climate projections through the  
40 Coupled Model Intercomparison Project [CMIP ; (Meehl et al., 2000)], an initiative of the World Climate Research  
41 Programme (WCRP). However, with a typical horizontal resolution of 50-250 km, GCMs have limited ability to  
42 simulate sub-grid weather (e.g., local variance, persistence, topography, etc.) and therefore cannot accurately  
43 define local-scale processes and feedbacks (e.g., deep convection, land-atmosphere interactions, etc.). This limits  
44 GCMs ability to simulate aspects of the present-day water cycle and to determine robust future changes for local  
45 and regional applications (Maraun and Widmann, 2018; Douville et al., 2021). RCMs dynamically downscale  
46 GCM outputs to create higher spatial resolutions of ~2 -50 km, providing richer regional spatial information (e.g.,  
47 small-scale processes and extreme events) for climate assessments and for impact and adaptation studies  
48 (Diaconescu and Laprise, 2013; Giorgi and Gao, 2018). However, such experiments are computationally  
49 expensive, so it is not practical to choose all GCMs for dynamical downscaling. Thus, a sub-set of GCMs has to  
50 be selected.

51 The WRCP's Coordinated Regional Climate Downscaling Experiment (Cordex) initiative delivers dynamically  
52 downscaled simulations of various GCMs (Giorgi and Gao, 2018) over 14 regions worldwide. This includes Phase  
53 I using CMIP5 (Giorgi et al., 2008) and Phase II Coordinated Output for Regional Evaluations (CORDEX-CORE)  
54 (Giorgi et al., 2021) as well as on-going experiments (CMIP6). However, there is no agreed approach to selecting  
55 which GCMs would be most suitable for dynamical downscaling, either in the recent WRCP's guideline for  
56 CMIP6 CORDEX experiments (Cordex, 2021) or across different CORDEX domains (Di Virgilio et al., 2022;  
57 Grose et al., 2023; Sobolowski et al., 2023). In the earliest initiatives, GCMs were eliminated based on their skill  
58 in reproducing the current climate for the region of interest given the fact that the bias in the GCMs can propagate  
59 into the RCM through the underlying and lateral boundary conditions (i.e., driven by initial and time-dependent  
60 meteorological variables from GCMs) (Mote et al., 2011; Overland et al., 2011; Mcsweeney et al., 2012;  
61 Mcsweeney et al., 2015). In addition, the selection of GCMs considers the need to generate a reasonable  
62 uncertainty range for future climate projections (Mote et al., 2011; Overland et al., 2011). Given the shared  
63 physical components of the design of CMIP6 GCMs, there are inherent biases in statistical properties like the  
64 multi-model mean or standard deviation of the full ensemble (Boé, 2018; Brands, 2022; Sobolowski et al., 2023).  
65 To address this problem, model dependency is also considered. These considerations and methodologies have  
66 been integrated into the most recent CMIP6 CORDEX experimental design for specific regions, such as Europe  
67 (Sobolowski et al., 2023) or Australia (Di Virgilio et al., 2022) and are recommended for widespread application  
68 across other CORDEX-domains.



69 Model evaluation is an essential part of CMIP6 model selection since simulating past performance well is a  
70 necessary (but insufficient) condition to have more confidence in future performance. Different metrics are  
71 employed to quantify model skill in simulating various climate variables at either global (Kim et al., 2020; Ridder  
72 et al., 2021; Wang et al., 2021b; Donat et al., 2023) or regional scales [e.g., Australia (Deng et al., 2021; Di  
73 Virgilio et al., 2022) Europe (Ossó et al., 2023; Palmer et al., 2023); South America (Díaz et al., 2021); Asia  
74 (Dong and Dong, 2021); Southeast Asia (Desmet and Ngo-Duc, 2022; Pimonsree et al., 2023)]. However, the lack  
75 of consistency in the list of metrics used makes it difficult to perform one-to-one comparisons between studies or  
76 to track model performance across various regions.

77 Recently, Isphording et al. (2024) introduced a standardised benchmarking framework (BMF) underpinned by the  
78 work of the U.S DOE (2020), which included a set of baseline performance metrics for assessing model  
79 performance in simulating different characteristics of rainfall. The BMF is different from traditional model  
80 evaluation in that it defines performance expectations a priori (Abramowitz, 2005; Abramowitz, 2012; Best, 2015;  
81 Nearing et al., 2018). Under the BMF, a model will not be considered fit-for-purpose if it fails any performance  
82 metric. The BMF consists of two tiers of metrics: the first tier includes minimum standard performance metrics  
83 related to fundamental characteristics of rainfall, and the second tier allows users to define metrics that help to  
84 answer specific scientific research questions. The BMF was initially designed for rainfall but can be widely  
85 applied to other climate variables (e.g., surface temperature), depending on the user's purpose (Isphording et al.,  
86 2024).

87 IPCC highlights Southeast Asia (SEA) as a region facing considerable climate change risks from extreme events  
88 (e.g., floods, extreme heat, and changing precipitation and extremes) (Ipcc, 2022). However, available regional  
89 climate simulations for SEA, particularly from CMIP5 CORDEX-SEA experiments are limited to 13 simulations  
90 (Tangang et al., 2020) compared to EURO-CORDEX with 68 simulations (Jacob et al., 2020) or CORDEX-  
91 Australasia with 20 simulations (Evans et al., 2021). Consequently, future projections come with a higher degree  
92 of uncertainty, especially for rainfall (Tangang et al., 2020; Nguyen et al., 2023). This motivated the CORDEX-  
93 SEA community to update their regional climate model simulations with the latest CMIP6 models. Note that over  
94 SEA, observations are sparse with large uncertainties, particularly for rainfall (Nguyen et al., 2020), making GCM  
95 evaluations more complicated (Nguyen et al., 2022; Nguyen et al., 2023). To date, the performance of various  
96 CMIP6 GCMs has been evaluated and ranked over the whole region of SEA (Desmet and Ngo-Duc, 2022;  
97 Pimonsree et al., 2023) and its sub-regions [e.g., Philippines (Ignacio-Reardon and Luo, 2023); Thailand  
98 (Kamworapan et al., 2021); Vietnam (Nguyen-Duy et al., 2023)]. Although there are groups of GCMs that  
99 consistently perform well (e.g., EC-Earth3, EC-Earth3-Veg, GFDL-ESM4, MPI-ESM1-2-HR, E3SM1-0,  
100 CESM2) and poorly (e.g., FGOALS-g3, CanESM, NESM3, IPSL-CM6A-LR) across available literature, their  
101 ranking varies differently given inconsistencies in evaluation metrics and observational reference datasets. This  
102 creates challenges in conducting direct intercomparisons across the above-mentioned studies. In addition, it is  
103 crucial to consider other important aspects discussed above (e.g., observational uncertainty, model dependency,  
104 and future climate change spread) in identifying the list of reliable models over SEA.

105 In this research, we aim to apply the lessons learnt from CMIP6 selection over different CORDEX-domains for  
106 SEA by assessing different aspects of models: model performance, model independence, data availability and  
107 future climate change spread. We apply the BMF to provide a consistent set of metrics for holistically evaluating



108 model performance and to deal with large observational uncertainties over the region. Focusing on precipitation,  
 109 where future projections are much more uncertain, the objectives of this research are twofold:

- 110 1. To evaluate the performance of CMIP6 GCMs in simulating the fundamental characteristics of  
 111 precipitation, its drivers and teleconnection with modes of variability over SEA using a standardised  
 112 benchmark framework and to identify a subset of models that meet our performance expectations.
- 113 2. To retain models that are relatively independent and are representative of the full range of possible  
 114 projected change for finalizing a subset of CMIP6 GCMs for dynamical downscaling over SEA using  
 115 model independence tests and assessment of climate change response patterns.

## 116 2 Methods

### 117 2.1 Data

#### 118 2.1.1 CMIP6 GCM data

119 We use the historical daily data of precipitation, near surface temperature, 850 hPa wind speed and both monthly  
 120 and daily sea-surface temperature data from the 32 CMIP6 models listed in Table 1. We consider models which  
 121 have a horizontal grid spacing greater than  $2^\circ \times 2^\circ$  to avoid the impact of the coarser GCMs on dynamical  
 122 downscaling. One simulation (typically the first member r1i1p1f1) is utilized in the benchmarking process to  
 123 enable a fair comparison. At the time of this analysis, the first member of some models (e.g., CNRM-family  
 124 models, UKESM1-0-LL).

125 **Table 1.** Information on model components from the CMIP6 GCMs used in this study.

No	Model	Run	Atmosphere lon/lat	Reference	Atmospheric component	Land component	Sea ice component	Ocean component
1	ACCESS-CM2	r1i1p1f1	$1.2^\circ \times 1.8^\circ$	Bi et al. (2020) and Ziehn et al. (2020)	UKMO UM v10.6	CABLE 2.5	LANL CICE5.1	MOM5
2	ACCESS-ESM1-5	r1i1p1f1	$1.2^\circ \times 1.8^\circ$		UKMO UM v7.3	CABLE2.4	LANL CICE4.1	GFDL MOM5
3	BCC-CSM2-MR	r1i1p1f1	$1.1^\circ \times 1.1^\circ$	Wu et al. (2019)	BCC-AGCM3	BCC-AVIM2	SIS4	MOM4-L40
4	CESM2	r1i1p1f1	$0.95^\circ \times 1.25^\circ$	Danabasoglu et al. (2020)	CAM6/WAC CM6	CLM5.0	CICE5	POP2
5	CMCC-CM2-HR4	r1i1p1f1	$0.95^\circ \times 1.25^\circ$	Cherchi et al. (2019)	CAM v5	CLM4.5	CICE4	NEMO v3.6
6	CMCC-CM2-SR5	r1i1p1f1	$0.9^\circ \times 0.9^\circ$					
7	CMCC-ESM2	r1i1p1f1	$0.95^\circ \times 1.25^\circ$					
8	CNRM-CM6-1	r1i1p1f2	$1.4^\circ \times 1.4^\circ$	Voldoire et al. (2019)	ARPPE-Climat v6.3	Flake	OASIS-MCT	NEMO
9	CNRM-CM6-1-HR	r1i1p1f2	$0.5^\circ \times 0.5^\circ$					
10	CNRM-ESM2-1	r1i1p1f2	$1.4^\circ \times 1.4^\circ$					
11	E3SM-1-0	r1i1p1f1	$1^\circ \times 1^\circ$	Zheng et al. (2022)	EAM (CAM 5.3)	MPAS-Ocean	MPAS-Seaice	ELMv0 (CLM4.5)
12	EC-Earth3-AerChem	r1i1p1f1	$0.7^\circ \times 0.9^\circ$	Döscher et al. (2022)	ECMWF IFS	LPJ-GUESS et al., 2013)	LIM3	NEMO v3.6
13	EC-Earth3-CC	r1i1p1f1	$0.7^\circ \times 0.9^\circ$					



No	Model	Run	Atmosphere lon/lat	Reference	Atmospheric component	Land component	Sea ice component	Ocean component
14	EC-Earth3	rli1plfl	0.7° × 0.7°					
15	EC-Earth3-Veg	rli1plfl	0.7° × 0.7°					
16	EC-Earth3-Veg-LR	rli1plfl	1.125° × 1.125°					
17	GFDL-CM4	rli1plfl	1.0° × 1.3°	Held et al. (2019); Dunne et al. (2020)	AM4	LM4	SIS 2	OM4 MOM6
18	GFDL-ESM4	rli1plfl	1.0° × 1.3°					
19	HadGEM3-GC31-MM	rli1plf3	0.9° × 0.9°	Andrews et al. (2020)	GA7/GL7		GSIS.1 (CICE5.1)	GO6 (NEMO)
20	INM-CM4-8	rli1plfl	1.5° × 2.0°	Volodin et al. (2017)	INM-AM4-8/5.0	INM-LND1	INM-ICE1	INM-OM5
21	INM-CM5-0	rli1plfl	1.5° × 2.0°					
22	IPSL-CM6A-LR	rli1plfl	1.3° × 2.5°	Boucher et al. (2020)	LMDZ 6A-LR	ORCHIDE 2.0	NEMO-LIM3.6	NEMO 3.6
23	IPSL-CM6A-LR-INCA	rli1plfl	1.27° × 2.5°					
24	MIROC6	rli1plfl	1.4° × 1.4°	Tatebe et al. (2019)	MIROC 3.2	MATSIRO	MIROC 3.2	COCO 4.5
25	MPI-ESM1-2-HR	rli1plfl	0.94° × 0.94°	Mauritsen et al. (2019)	ECHAM6.3	JSBACH)	MPIOM	
26	MPI-ESM1-2-LR	rli1plfl	1.875° × 1.875°					
27	MRI-ESM2-0	rli1plfl	1.1° × 1.1°	Yukimoto et al. (2019)	MRI-AGCM3.5		MRI.COMv4	
28	NESM3	rli1plfl	1.9° × 1.9°	Cao et al. (2018)	ECHAM6.3	JSBACH	CICE4	NEMO v3.4
29	NorESM2-MM	rli1plfl	0.9 × 0.9°	Seland et al. (2020)	CAM4-Oslo	CLM4	CICE4	MICOM
30	SAM0-UNICON	rli1plfl	0.9° × 1.3°	Park et al. (2019)	CAM5.3 with UNICON	CLM4	CICE4.0	POP2
31	TaiESM1	rli1plfl	0.9° × 0.9°	Wang et al. (2021a)	Tai AM1	CLM4.0	CICE4	POP2
32	UKESM1-0-LL	rli1plf2	1.3° × 1.9°	Sellar et al. (2019)	MetUM-HadGEM3-GA7.1	JULES-ES-1.0	CICE-HadGEM3-GSIS	NEMO-HadGEM3-GO6.0

126 **2.1.2 Observations and reanalyses**

127 Given the large observational uncertainty in precipitation over the region (Nguyen et al. 2022), we use multiple  
 128 daily observed datasets from different in situ and satellite sources to quantify model skill (Table 2). These datasets  
 129 have been chosen given their high consistency in representing daily precipitation (Nguyen et al., 2022) and  
 130 extremes (Alexander et al., 2020; Nguyen et al., 2020) over SEA.

131 ERA5 reanalysis (Hersbach et al., 2020) was used to benchmark model performance in representing the  
 132 climatology of atmospheric circulation (e.g., metrics related to horizontal wind at 850 hPa level are described in  
 133 section 2.2).

134 We acknowledge that different observational sea surface temperatures (SST) have different abilities to capture  
 135 signals of the modes of variability. Therefore, we utilize multiple SST products (Table 2) to take account of the



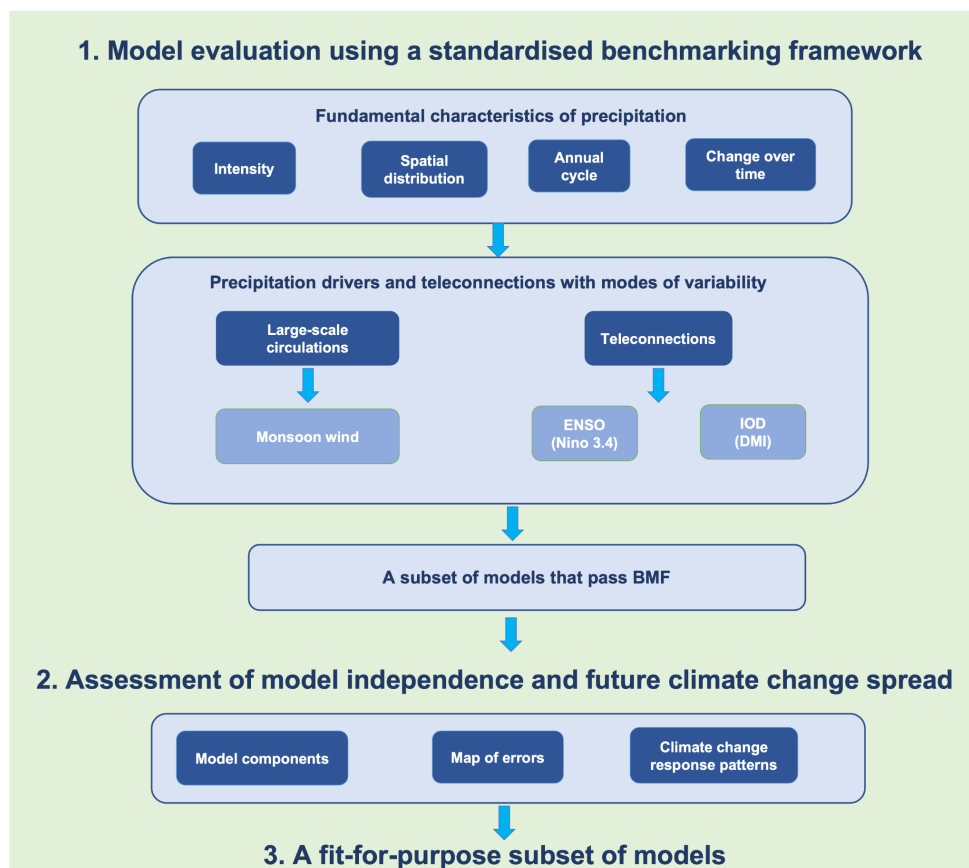
136 observational uncertainties in simulating the teleconnection between rainfall and main modes of variability,  
 137 including El Niño-Southern Oscillation (ENSO) and Indian Ocean Dipole (IOD) as described in section 2.2.

138 **Table 2.** The main characteristic of observational datasets used in this study.

Type of dataset	Product short name	Dataset name	Temporal coverage	Spatial resolution	Data source	Reference
Precipitation dataset	APHRODITE	APHRODITE V1101 and V1101XR	1950-2015	0.5° × 0.5°	In situ	Yatagai et al. (2012)
	CHIRPv2	CHIRPSv2	1981-2016	0.25° × 0.25°	In situ + Satellite	Funk et al. (2015)
	REGEN_ALL	REGEN Allstns V1 2019	1950-2019	1° × 1°	In situ	Contractor et al. (2020)
	GPCC_v2018	GPCC FDD v2018	1982-2019	1° × 1°	In situ	Schamm et al. (2014)
Sea Surface Temperature dataset	HadISST	HadISST1 v1	1870-2021	1° × 1°	In situ + Satellite	Rayner et al. (2003)
	OISST	OISST v2.0	1981-2020	0.25° × 0.25°	In situ + Satellite	Huang et al. (2021)
	ERSST	ERSST v5	1854-2024	2° × 2°	In situ	Huang et al. (2017)

139 **2.2 Benchmarking CMIP6 GCMs over Southeast Asia**

140 Given the large uncertainties and model inconsistency in rainfall projections, our main aim is to identify a subset  
 141 of CMIP6 GCMs that meet our a priori expectations. That is, as a minimum requirement a model should simulate  
 142 past rainfall statistics over SEA reasonably well using consistent criteria. Figure 1 illustrates the GCM selection  
 143 process applied in this research based on a standardised benchmarking framework (Isphording et al., 2024). A  
 144 subset of CMIP6 GCMs that meet our model performance expectations are identified through a two-step process:  
 145 (a) selecting models that meet minimum performance requirements in simulating the fundamental characteristics  
 146 of rainfall (Fig. 1) and (b) selecting models from (a) to further assess performance in simulating precipitation  
 147 drivers (e.g., monsoon) and teleconnections with modes of variability (Fig. 1).



148

149 **Figure 1.** A schematic of the CMIP6 GCM selection process, including (1) model evaluation using a standardized  
150 benchmarking framework (BMF) and (2) assessment of model independence and future climate change spread. The BMF  
151 includes two steps: minimum standard metrics (MSMs) which assess very basic characteristics of rainfall and second-tier  
152 metrics (e.g., versatility metrics) which quantify model skill of the models that pass the MSMs in simulating precipitation  
153 drivers (monsoon) and teleconnections with modes of variability [the El Niño-Southern Oscillation (ENSO) and Indian Ocean  
154 Dipole (IOD)].

### 155 2.2.2 Versatility metrics

156 The MSMs provide statistical measurements that are not always correlated with future projections (Knutti et al.,  
157 2010), given that some models may simulate historical precipitation well for the wrong reasons. A further  
158 recommendation is therefore to also assess model performance based on key physical processes (Doe, 2020;  
159 Nguyen et al., 2023). This approach offers additional insights into the relative roles of model biases in simulating  
160 large-scale environments versus the limitations of model parameterizations in generating precipitation biases.  
161 Therefore, we define second tier versatility metrics to assess those GCMs selected from section 2.2.1 in simulating  
162 the complex precipitation-related processes, including drivers and teleconnections with modes of variability.

#### 163 Monsoon circulation

164 SEA is situated within the Asian monsoon regime, where atmospheric circulation is modulated by two primary  
165 monsoon systems: the Indian monsoon characterized by westerlies from the Bay of Bengal into northern parts of



166 SEA including the mainland and northern Philippines (along 10°N) during the boreal summer (JJAS) and reversed  
167 in direction during the boreal winter (DJF); and the Australian monsoon [e.g., easterlies from Australia to the  
168 Maritime Continent (MC) and Papua] (Chang et al., 2005). These monsoon systems drive regional rainfall  
169 seasonality. Therefore, we focus on assessing model skill in simulating the intensity and direction of monsoon  
170 wind (e.g., 850-hPa wind) for JJAS and DJF. While wind speed is evaluated using the MAPE and Scor metrics  
171 similar to the MSMs for precipitation and temperature, wind direction is quantified using an equation from Desmet  
172 and Ngo-Duc (2022):

$$173 \text{ MD} = \frac{\sum_i u_i \times |\theta_i - \theta_{i,ref}|_{[0,180]}}{\sum_i u_i}$$

174 where  $u_i$ ,  $\theta_i$ ,  $\theta_{ref}$  refer to the simulated wind speed at the grid  $i$ ,  $|\theta_i - \theta_{i,ref}|_{[0,180]}$  is the absolute value of  
175 difference at the  $i$ th grid between directions of simulated and reference wind speed (e.g., ERA5). The MD metric  
176 allows us to quantify the agreement in wind direction between two datasets in which the impact of high wind  
177 speed is taken into account.

#### 178 ENSO, IOD and Teleconnections

179 Various parts of SEA are also affected by two prominent modes of variability: the El Niño - Southern Oscillation  
180 (ENSO) (Haylock and McBride, 2001; Chang et al., 2005; Juneng and Tangang, 2005; Qian et al., 2013) and Indian  
181 Ocean Dipole (IOD) (Xu et al., 2021) via atmospheric teleconnections. In this research, the teleconnection is  
182 defined by the temporal correlation between precipitation anomalies at each grid point and the respective  
183 Niño3.4/IOD region.

184 Since ENSO typically matures toward the end of the calendar year (Rasmusson and Carpenter, 1982), we consider  
185 ENSO developing years as year (0) and use the DJF means to identify ENSO events. Over SEA, ENSO interacts  
186 with the monsoon cycle and due to the varying monsoon onset between the northern and southern parts of the  
187 region, its seasonal evolution differs across regions. In particular, there is a lagged negative correlation between  
188 rainfall and ENSO over the Maritime Continent (MC) and the Philippines, which develops from May-June,  
189 strengthens during July-August, and reaches its highest correlation during September-October of the developing  
190 year (year 0). On the other hand, this negative correlation becomes prominent over the northern parts during the  
191 subsequent boreal spring (from March-May of the year +1) (Wang et al., 2020; Chen et al., 2023). The negative  
192 correlation indicates dry anomalies during El Niño and/or wet anomalies during La Nina. Therefore, in the context  
193 of this research, we examine the lead/lag Pearson correlation of the DJF Niño3.4 index in the developing year  
194 (year 0) with two different seasonal rainfalls: May-Oct (MJJASO) of the developing year (year 0) and March-  
195 May (MAM) of the following year (year +1).

196 Furthermore, considering the stronger influence of the IOD and its associated teleconnection during SON  
197 compared to other seasons (Mckenna et al., 2020), we calculated the in-phase Pearson correlation coefficient  
198 between the detrended precipitation anomaly and DMI for the SON season. The statistical significance of the  
199 correlation coefficient is tested using the Student t-test ( $\alpha = 0.05$ ). Note that IOD could exist as part of ENSO  
200 (Allan et al., 2001; Baquero-Bernal et al., 2002) and their coexistence could have strong impacts on rainfall  
201 variability over many parts of SEA (D'arrigo and Wilson, 2008; Amirudin et al., 2020), which is not investigated  
202 in this study.





203 To track ENSO variability, the Niño3.4 index (5°S-5°N and 160°E-120°W) (Trenberth and Hoar, 1997; Shukla et  
204 al., 2011) derived for the 1951-2014 period as area-mean monthly SST anomalies with respect to a 1961-1990  
205 climatology is used. For IOD, we use the Dipole Mode Index [DMI; (Saji et al., 1999; Meyers et al., 2007)] DMI  
206 measures differences of monthly SST anomalies between the west equatorial Indian Ocean (50-70° E, 10°S-10°N)  
207 and those in the east (90-110°S, 10°S -0°N). We use a 5-monthly average Niño3.4 and IOD index to remove  
208 seasonal cycles. The resulting month time series are detrended using a fourth-order polynomial fit to remove the  
209 possible influence of a long-term trend and to better preserve high amplitude (<10 years) variability (Braganza et  
210 al., 2003).

211 Previous literature has often focused on assessing the robustness of rainfall teleconnections (e.g., spatial patterns  
212 and amplitudes) across CMIP model ensembles. These assessments typically involve examining agreement in the  
213 sign of teleconnections such as through rainfall anomaly composites (Langenbrunner and Neelin, 2013) and  
214 regional average teleconnection strength over land (Perry et al., 2020) or a combination of both (Power and  
215 Delage, 2018) rather than evaluating the skill of an individual model. However, since rainfall teleconnections  
216 across SEA exhibit spatial and seasonal variability, the above metrics may be substantially influenced by internal  
217 variability. For high level qualification, we employ spatial correlation and simplified metrics for assessing  
218 agreement in the significant sign of the teleconnections, as recommended by Liu et al. (2024). We assess the  
219 similarity in the number of grid points detecting significant signals between observed and modelled  
220 teleconnections using a set of three metrics: Hit rate (HR), Miss Rate (MR) and False Alarm rate (FAR) as follows:

$$221 \text{ HR} = \frac{\text{Area with correct sign of significant correlation}}{\text{Area with significant correlation in OBS}} \times 100 (\%)$$

$$222 \text{ MR} = \frac{\text{Area with significant correlation in OBS but with no significant correlation in model}}{\text{Area with significant correlation in OBS}} \times 100 (\%)$$

$$223 \text{ FAR} = \frac{\text{Area with no significant correlation in OBS but with significant correlation in model}}{\text{Area with no significant correlation in OBS}} \times 100 (\%)$$

224 These metrics allow us to make sure that the model adequately simulates significant signals across the entire  
225 region. While HR ranges from 0-100 %, MR and FAR vary. A desirable model outcome includes a high HR value  
226 coupled with a low MR and FAR value, indicating the model's ability to adequately capture the significance of  
227 the correct signal in the right region (on grid scales) of teleconnections between ENSO and IOD and rainfall  
228 pattern.

### 229 2.3. GCM independence assessment and future climate change spread

230 Model independence could be assessed based on model components (e.g., shared atmospheric, land, and/or ocean  
231 models) and/or model output patterns. In this study, we employ both methods for testing GCM independence.  
232 Table 1 provides information on the principal components of the models used in this study. Note that model  
233 independence based on this criterion could depend on the model version (e.g., the same model with different levels  
234 of complexity). In addition, we acknowledge that the spatial pattern of error maps and future changes maps seem  
235 to correlate well with model dependency (Knutti et al., 2010; Knutti and Sedláček, 2013; Brunner et al., 2020;  
236 Brands, 2022). Therefore, we determine the independence of GCMs simply by calculating the correlation  
237 coefficient of historical biases and future projections between models and then apply a hierarchical clustering  
238 approach (Rousseeuw, 1987) to this correlation matrix to group models. This cluster analysis has been employed  
239 in previous literature for multiple purposes, e.g., to assess model dependency (Brunner et al., 2020; Masson and



240 Knutti, 2011), spatial patterns of climatology and trends in climate extremes (Gibson et al., 2017) or spatial pattern  
241 of precipitation change signals (Gibson et al., 2024).

242 Note that historical biases are calculated by comparing the climatology of total rainfall over the land area of SEA  
243 for the 1951-2014 period with corresponding data from an observed reference. Meanwhile, for future signals, we  
244 focus on the relative change (in percentage) between the far future (2070-2099) and the baseline (1961-1990) as  
245 suggested by the World Meteorological Organization (WMO). All analyses are conducted for two seasonal  
246 periods: wet MJJASO and dry NDJFMA seasons.

247 We use the coarsest resolution (i.e., NESM  $\sim 216$  km or  $1.9^\circ \times 1.9^\circ$  resolution) among 32 GCMs as the target  
248 resolution for comparison. All data are interpolated into a spatial resolution of  $1.9^\circ \times 1.9^\circ$  using a first-order  
249 conservative regridding method (Jones, 1999) to better capture the spatial discontinuity of precipitation  
250 ((Contractor et al., 2018).

251 Benchmarking CMIP6 GCMs against observations is conducted over land for precipitation and the  
252 teleconnections between precipitation and modes of variability while 850-hPa winds from ERA5 allow the  
253 comparison to also be extended over the ocean.

254 Hereafter, we select APHRODITE as the primary baseline for all the main figures, as it utilises the greatest number  
255 of rain gauges of any dataset. We include the results related to all other observational datasets in the  
256 Supplementary section (Fig. s1-5) and provide a detailed explanation of related results in the main text for  
257 intercomparison purposes.

## 258 **3 Results**

### 259 **3.1 Minimum Standard Metrics (MSMs)**

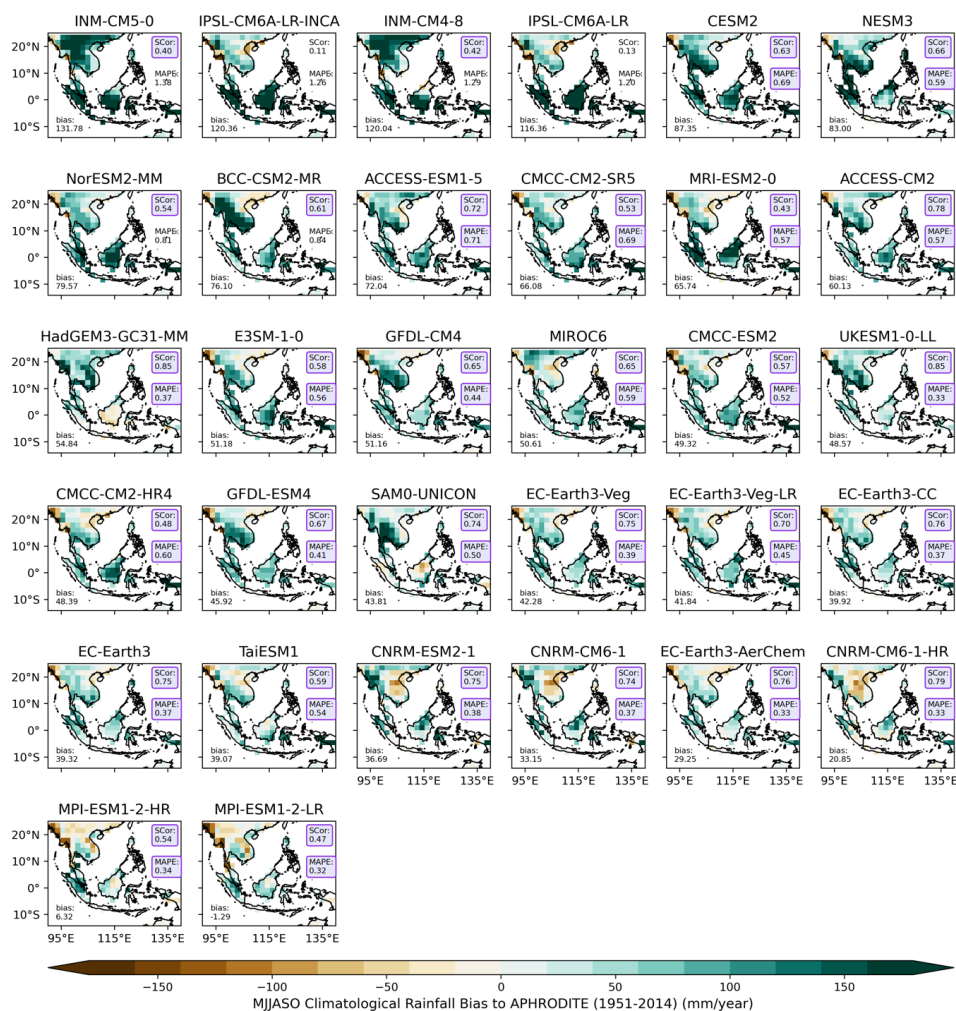
#### 260 **3.1.1 MAPE and Spatial correlation (Scor)**

261 We initially assess the performance of CMIP6 GCMs in reproducing the spatial distribution of precipitation, using  
262 the first two MSMs: MAPE and Scor. Previous studies have emphasized strong seasonal and regional contrasts in  
263 rainfall distribution over Southeast Asia (Nguyen et al., 2023). Therefore, we focus on comparing the seasonal  
264 climatology (1951-2014) of total rainfall during wet days (e.g., precipitation  $\geq 1$ mm) between models and  
265 APHRODITE for both wet MJJASO and dry NDJFMA seasons (Fig. 2 and Fig. 3 respectively). For MSMs, our  
266 strategy is to retain as many models as possible. We establish benchmarking thresholds based on the requirements  
267 of downscaling CMIP6 from CORDEX communities and our understanding of reasonable model performance  
268 based on current scientific understanding. In particular, GCMs should adequately produce the spatial distribution  
269 of rainfall and without a strong wet or dry bias. In addition, we also identify observational uncertainties through  
270 inter-comparison of multiple precipitation datasets. Considering variations in model performance across seasons,  
271 we also set different thresholds for benchmarking models for different seasons. In particular, due to a better  
272 model's ability to capture spatial variability of precipitation during the dry season compared to the wet season  
273 (Desmet and Ngo-Duc, 2022), we adopt a more lenient approach by relaxing our expectation for a spatial  
274 distribution metric, setting the Scor threshold  $\geq 0.4$  for the wet season and  $\geq 0.75$  for the dry season. However,  
275 for the MAPE score, we apply a stricter criterion, as we require models to closely simulate observed rainfall



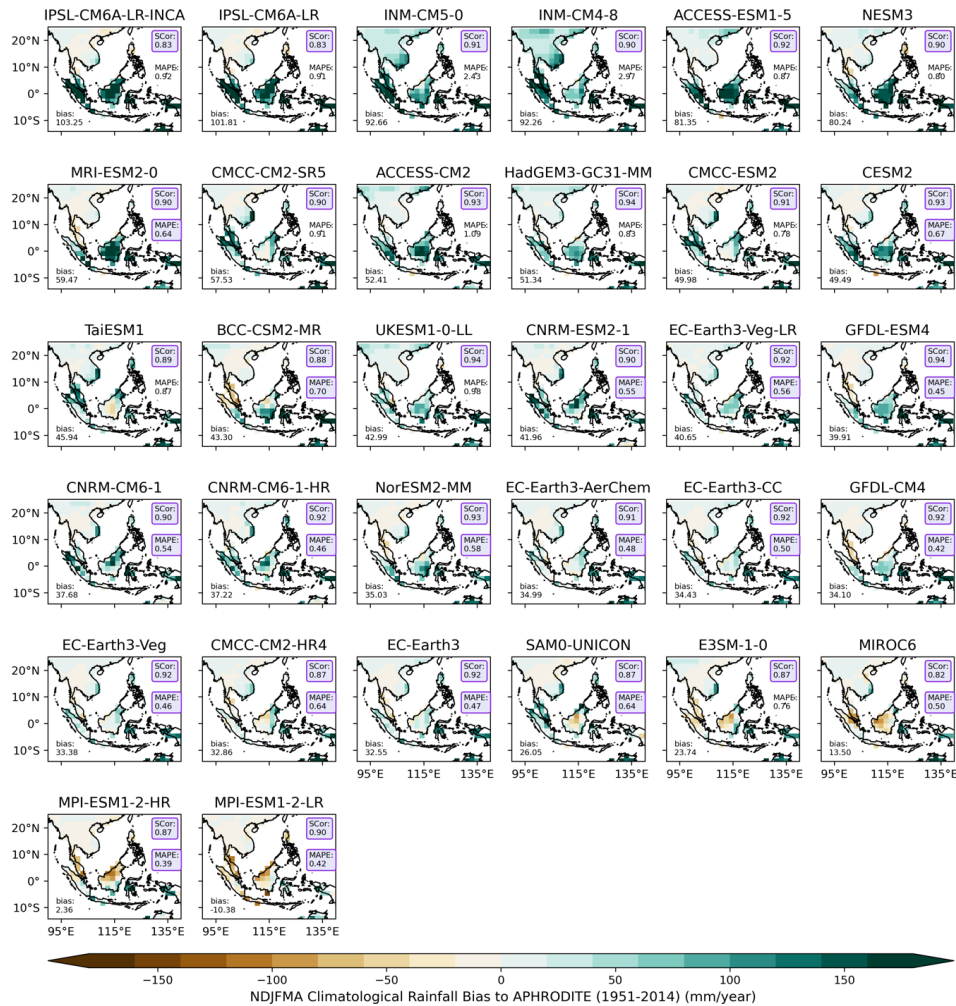
276 intensity over SEA. For both wet and dry seasons, we set the benchmarking threshold for MAPE at  $\leq 0.75$ . With  
277 this threshold, our objective is to identify models capable of capturing the spatial variability of rainfall across at  
278 least 40% ( $\text{Scor} \geq 0.4$ ) or 75% ( $\text{Scor} \geq 0.75$ ) of the domain during wet and dry seasons respectively, with a  
279 wet/dry bias of no more than 75% compared to observations ( $\text{MAPE} \leq 0.75$ ) for both seasons.

280 We first discuss key features of the wet season (MJJASO; Fig. 2). Models are ranked from wettest to driest based  
281 on their regionally-averaged climatologies. Models that meet our benchmarking thresholds for MAPE and Scor  
282 (i.e., calculated against APHRODITE) are highlighted by purple-coloured boxes. In general, CMIP6 GCMs  
283 demonstrate a wet bias in terms of regional averages, ranging from 6.32 mm/year to 131.78 mm/year except for  
284 MPI-ESM1-2-LR (-1.29 mm/year). However, there is spatial variability in the distribution of wet and dry biases.  
285 While most of these models consistently show wet biases over MC, dry biases are observed in different locations  
286 on the mainland across models [e.g., along the west coast (e.g., EC-Earth, IPSL and CMCC families) or east coast  
287 (e.g., CNRM family) as well as in some northern regions (e.g., MPI family)]. Among the wettest GCMs, including  
288 INM, IPSL, NorESM2-MM and CESM2 family, the largest biases are predominantly over MC. Interestingly,  
289 most CMIP6 GCMs can capture the spatial variability of rainfall (Scor is around or greater than 0.5), except for  
290 the IPSL-family simulations (Scors of 0.11 and 0.13). Using the threshold definitions mentioned above, six models  
291 fail to meet these benchmarks, exhibiting obvious grouping by GCM group. For example, IPSL-CM6A-LR and  
292 IPSL-CM6A-LR-INCA fail due to their low Scor (0.13 and 0.11 respectively) and high MAPE (1.20 and 1.26  
293 respectively). While INM-CM5-0 and INM-CM4-8 models meet our set expectation in relation to spatial  
294 variability, they fail to meet the MAPE threshold due to their overestimation of rainfall across the entire region  
295 (e.g., MAPE ranging from 1.29 to 1.38 respectively). All mentioned failed models exhibit high MAPE values,  
296 ranging from 0.81 to 1.28.



297

298 **Figure 2.** The seasonal climatological (1951-2014) bias (in mm/year) for each model against the APHRODITE observational  
 299 product during the wet season (May-October; MJJASO), ranked wettest to driest based on regionally-averaged bias. The mean  
 300 absolute percentage error (MAPE) and spatial correlation (Scorr) calculated against APHRODITE are shown in the upper right  
 301 corner. Values highlighted in purple-coloured boxes indicate values that meet our defined benchmarking thresholds. All  
 302 analyses are considered at the resolution of the coarsest CMIP6 GCM (i.e., NESM3, ~ 216km).



303  
 304

**Figure 3.** Same as figure 2 but for the dry season (Nov-April; NDJFMA).

305  
 306  
 307  
 308  
 309  
 310  
 311  
 312  
 313  
 314

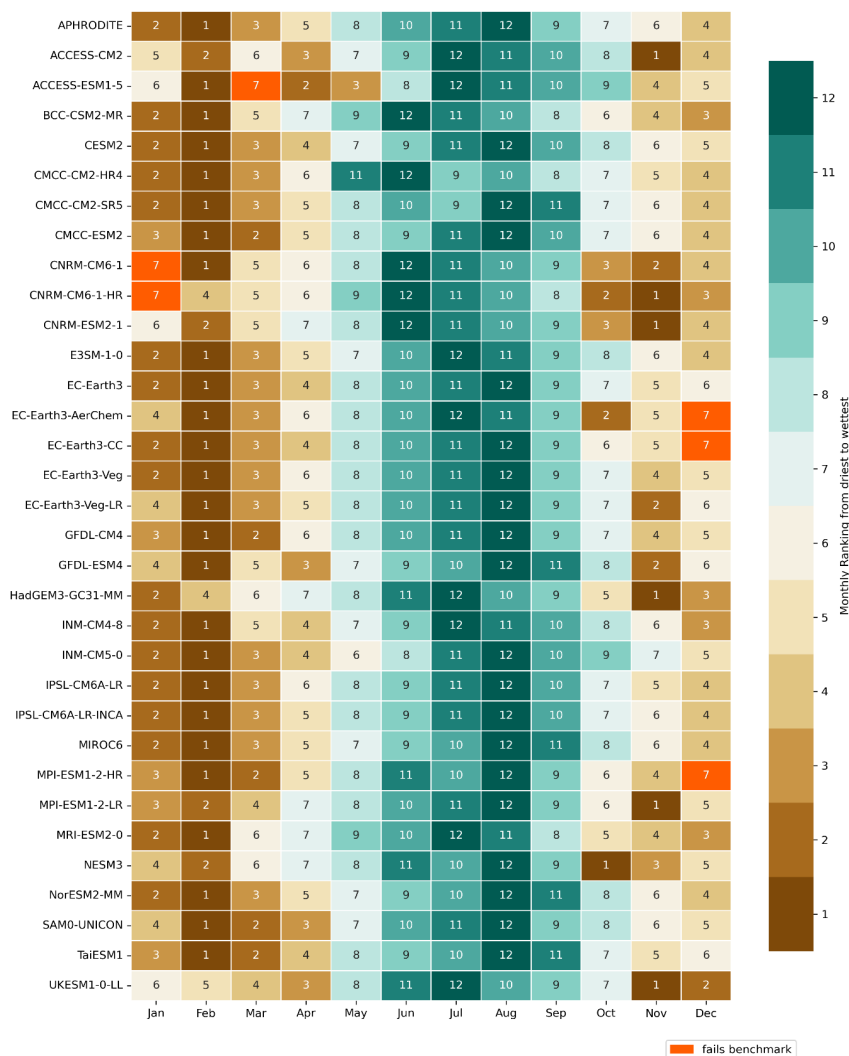
The corresponding results for the dry season reveal some interesting features (Fig. 3). First, there are substantial similarities in the spatial distribution of climatological rainfall biases across models during this season. CMIP6 GCMs consistently show small biases over Indochina and large wet biases over MC. Consequently, a better spatial correlation with observations (i.e., Scor > 0.8) is obtained during the dry season, consistent with previous findings [e.g., CORDEX-CMIP5 RCMs (Nguyen et al., 2022) or CMIP6 GCMs (Desmet and Ngo-Duc, 2022)] in highlighting the dependence of model performance on the season. With improved performance in capturing the spatial variation of total precipitation intensity compared to the wet season, all models meet our expected performance in spatial variability. However, INM- and IPSL-family models still fail the MAPE criterion since they exhibit much higher precipitation intensity than APHRODITE, particularly over MC. Note that over SEA, APHRODITE is drier than other precipitation products particularly over MC (Nguyen et al., 2020).



315 It is important to note that whether a model passes or fails the benchmarking is strongly dependent on the choice  
 316 of threshold as emphasised in Ispording et al. (2024). For instance, more simulations would fail this test if we  
 317 set a higher threshold of Scor, notably for the MJJASO season case.

### 318 3.1.2. Seasonal cycle

319 In this section, we follow the simplified method developed by Ispording et al. (2024) in quantifying the phase  
 320 and structure of the seasonal cycle. In particular, we rank total monthly precipitation from wettest to driest and  
 321 define the benchmarking threshold as the four wettest and driest observed months must be among the six wettest  
 322 and driest modelled months (Fig. 4).



323

324 **Figure 4.** The climatological (1951-2014), average total monthly rainfall over the mainland Southeast Asia are ranked from  
 325 driest to wettest for each CMIP6 simulation. Brown shades (1-6) indicate the six driest months while teal colours (7-12)



326 indicate the six wettest months. The models failed in benchmarking are highlighted in orange colour. All analyses are  
327 considered at the coarsest CMIP6 GCM (i.e., NESM3, ~ 216km).

328 Overall, most CMIP6 GCMs reproduce the phase well but tend to overestimate precipitation intensity, notably for  
329 the observed precipitation peaks during boreal summer (Fig. s1). The INM- and IPSL-family simulations stand  
330 out, consistent with the wettest biases observed in spatial patterns (section 3.1.1).

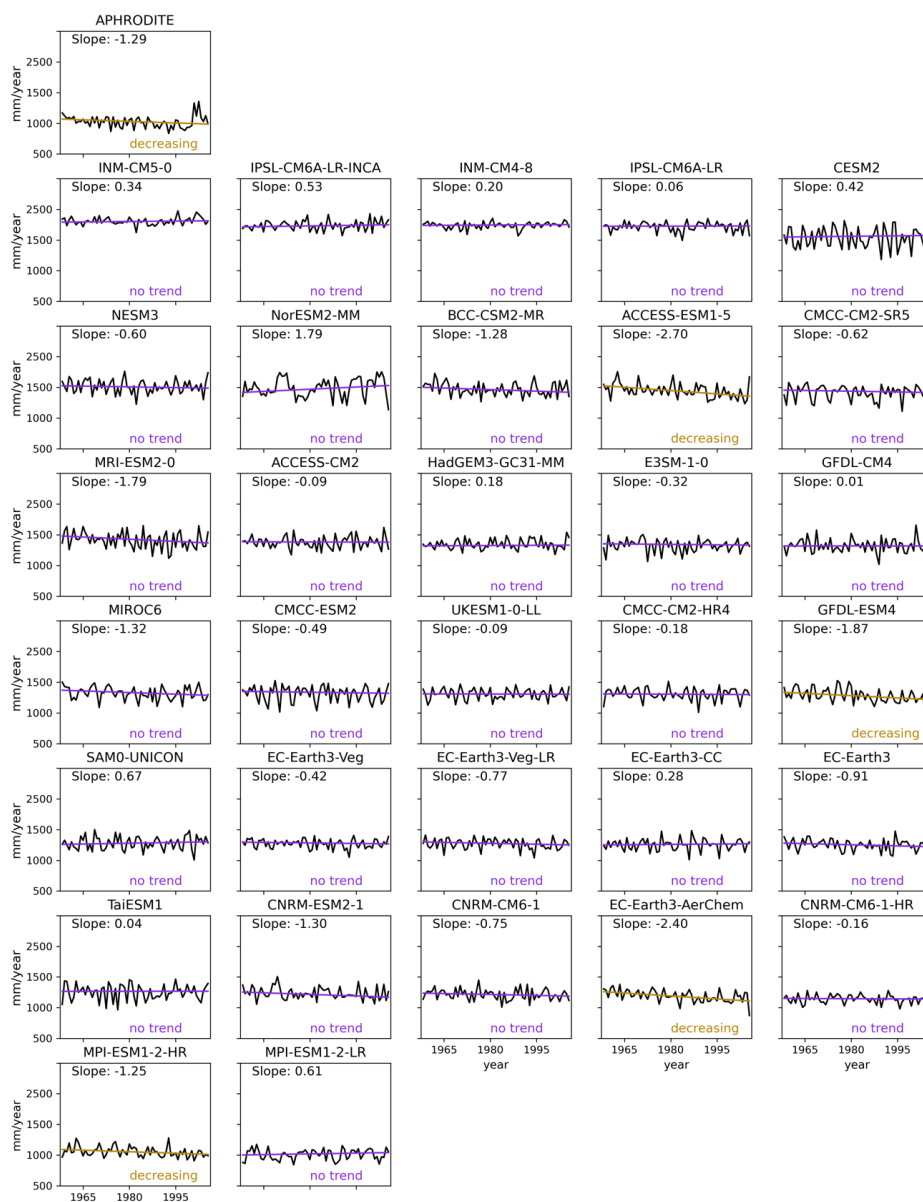
331 According to the benchmarking threshold definitions, all models pass the benchmarking regarding the four wettest  
332 observed months. However, six models fail the benchmark in terms of the four driest observed months  
333 (highlighted in orange in Fig.4). These models have their sixth wettest month (ranked as 7 in Fig. 4) falling within  
334 the APHRODITE's driest four months (Dec-Mar).

### 335 3.1.3. Significant trend

336 The final MSM aims to explore how rainfall changes over time (Isphording et al., 2024). In this part, we compare  
337 the direction of significant simulated and observed trends using the seasonal [wet season (Fig. 5)] and dry season  
338 (Fig. 6)] total precipitation. A Theil-Sen trend is calculated over a 65-year period (1951-2014) and tested at a 5%  
339 significance level using a Mann-Kendall significant test (Kendall, 1975).

340 There is no significant trend in observed total precipitation during the wet season while the dry season sees a  
341 significant increase trend. A model fails this benchmark if it exhibits an opposite significant trend to that of the  
342 observations. Using this definition, all models pass this benchmark during the wet season, but MRI-ESM2-0 and  
343 MPI-ESM-1-2-HR fail during the dry season.

344 Note that AR6 [Chapter 8 (Douville et al., 2021)] stated much more confidence in precipitation trends over MC  
345 after 1980. Therefore, we conducted an additional trend calculation (figures not shown) over the 33-year (1982-  
346 2014) period for all considered observational products. Although there are differences in the slope of changes  
347 among observational products, their direction (not shown) remains the same as the 1951-2014 period.

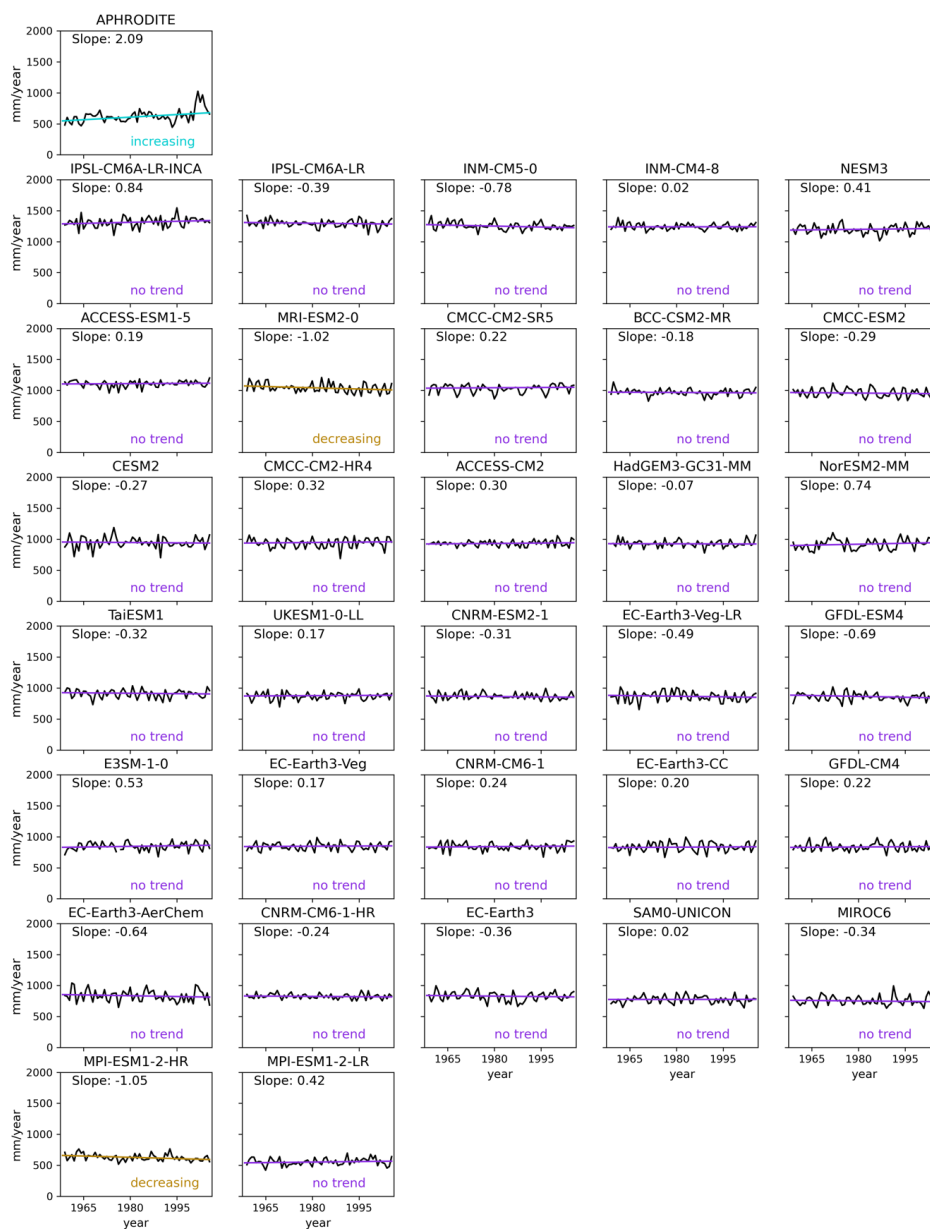


348

349 **Figure 5.** The observed (top row) and modelled seasonal average total precipitation across Southeast Asia land areas during  
 350 the wet season (May-October, MJJASO) for the period 1951-2014. The direction of the observed Thiel-Sen trend is the  
 351 benchmark (top row). The Thiel-Sen trend line for each of the simulations is plotted in grey if the models fail the benchmark  
 352 and in purple if they pass. The magnitude of the trend is noted in the top middle corner and the results of the Mann-Kendall  
 353 significance test is noted in the bottom right corner. Models are sorted based on the magnitude of the spatial average to match  
 354 the order of Figure 2. All analyses are considered at the coarsest CMIP6 GCM (i.e., NESM3, ~ 216km). All models pass the  
 355 benchmark.

356





357

358 **Figure 6.** Same as Figure 5 but for the boreal dry season (November – April, NDJFMA).

359 Table 3 summarizes the MSM benchmarking results for the 32 CMIP6 GCMs tested. There are 19 simulations  
 360 that pass all MSMs and therefore meet the minimum requirements for the purpose of this study.



361 **Table 3.** Summary of model performance against the MSMs for precipitation. Models fail where the benchmarks are  
 362 highlighted in red.

Simulations	Wet season		Dry season		Seasonal cycle	Trend		Pass/7
	MAPE	Scor	MAPE	Scor		Wet	Dry	
ACCESS-CM2	+	+	+	+	+	+	+	7
ACCESS-ESM1-5	+	+	+	+	-	+	+	6
BCC-CSM2-MR	+	+	+	+	+	+	+	7
CESM2	+	+	+	+	+	+	+	7
CMCC-CM2-HR4	+	+	+	+	+	+	+	7
CMCC-CM2-SR5	+	+	+	+	+	+	+	7
CMCC-ESM2	+	+	+	+	+	+	+	7
CNRM-CM6-1	+	+	+	+	-	+	+	6
CNRM-CM6-1-HR	+	+	+	+	-	+	+	6
CNRM-ESM2-1	+	+	+	+	+	+	+	7
E3SM-1-0	+	+	+	+	+	+	+	7
EC-Earth3-AerChem	+	+	+	+	-	+	+	6
EC-Earth3-CC	+	+	+	+	-	+	+	6
EC-Earth3	+	+	+	+	+	+	+	7
EC-Earth3-Veg	+	+	+	+	+	+	+	7
EC-Earth3-Veg-LR	+	+	+	+	+	+	+	7
GFDL-CM4	+	+	+	+	+	+	+	7
GFDL-ESM4	+	+	+	+	+	+	+	7
HadGEM3-GC31-MM	+	+	+	+	+	+	+	7
INM-CM4-8	-	+	-	+	+	+	+	5
INM-CM5-0	-	+	-	+	+	+	+	5
IPSL-CM6A-LR	-	-	-	+	+	+	+	4
IPSL-CM6A-LR-INCA	-	-	-	+	+	+	+	4
MIROC6	+	+	+	+	+	+	+	7
MPI-ESM1-2-HR	+	+	+	+	-	+	-	5
MPI-ESM1-2-LR	+	+	+	+	+	+	+	7
MRI-ESM2-0	+	-	+	+	+	+	+	6
NESM3	+	+	-	+	+	+	+	5
NorESM2-MM	-	+	+	+	+	+	+	6
SAM0-UNICON	+	+	+	+	+	+	+	7
TaiESM1	+	+	+	+	+	+	+	7
UKESM1-0-LL	+	+	+	+	+	+	+	7



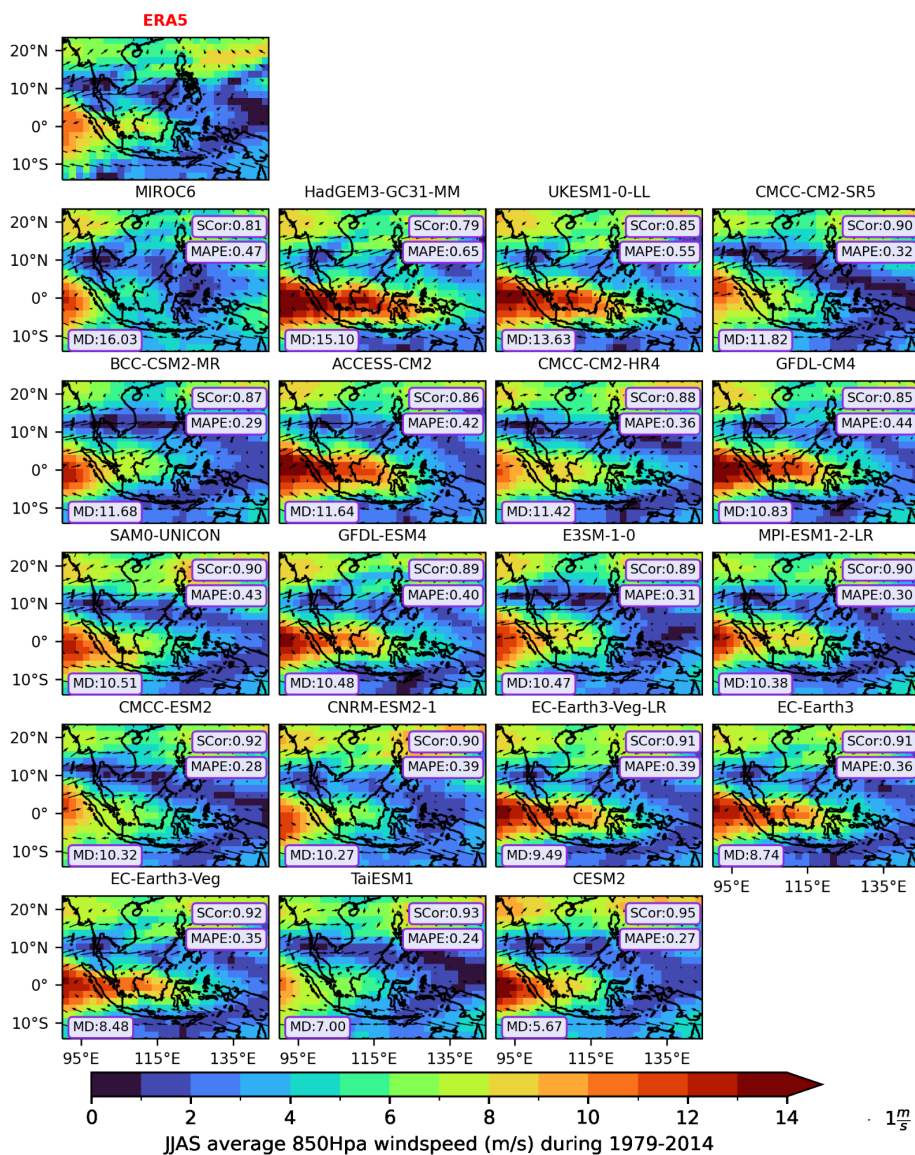
363 While the BMF was designed for precipitation, we can also apply the MSMs to other climate variables such as  
364 annual mean near-surface temperature (see Supplementary Fig. s2-4 and Tables s1-2). For temperature, we use  
365 the APHRODITE daily temperature datasets [version V1204R1 and V1204XR (Yatagai et al., 2012)] that span  
366 1961–2015. In general, CMIP6 GCMs show biases of variable sign for average temperature, with a greater number  
367 of GCMs exhibiting cold biases rather than warm biases (Fig. s2). Almost all models succeed in simulating the  
368 observed spatial distribution (e.g., Scor greater than 0.75), phases (e.g., no model fails the benchmarking for  
369 temperature cycle, Table s1) and historical trends (e.g., increase trend, Fig. s5) of temperature. Overall, models  
370 are better at simulating temperature characteristics (e.g., spatial pattern, annual cycle, and trend) than precipitation  
371 over SEA. Out of four models that fail the MSMs for near-surface temperature, two INM-family simulations do  
372 not meet the expected spatial distribution benchmark ( $\text{Scor} \geq 0.85$ ) while CNRM-CM6-1-HR and NESM3 show  
373 the largest relative errors compared to APHRODITE ( $\text{MAPE} = 0.08$ ). These four models also fail in MSMs for  
374 precipitation, as discussed above.

### 375 **3.2 Versatility metrics – Process-oriented metrics**

376 In addition to the MSMs, our aim is to select a subset of GCMs for dynamical downscaling that simulate  
377 precipitation mechanisms. Therefore, in the next steps we focus on process-oriented metrics which capture the  
378 relationship between precipitation and other variables well.

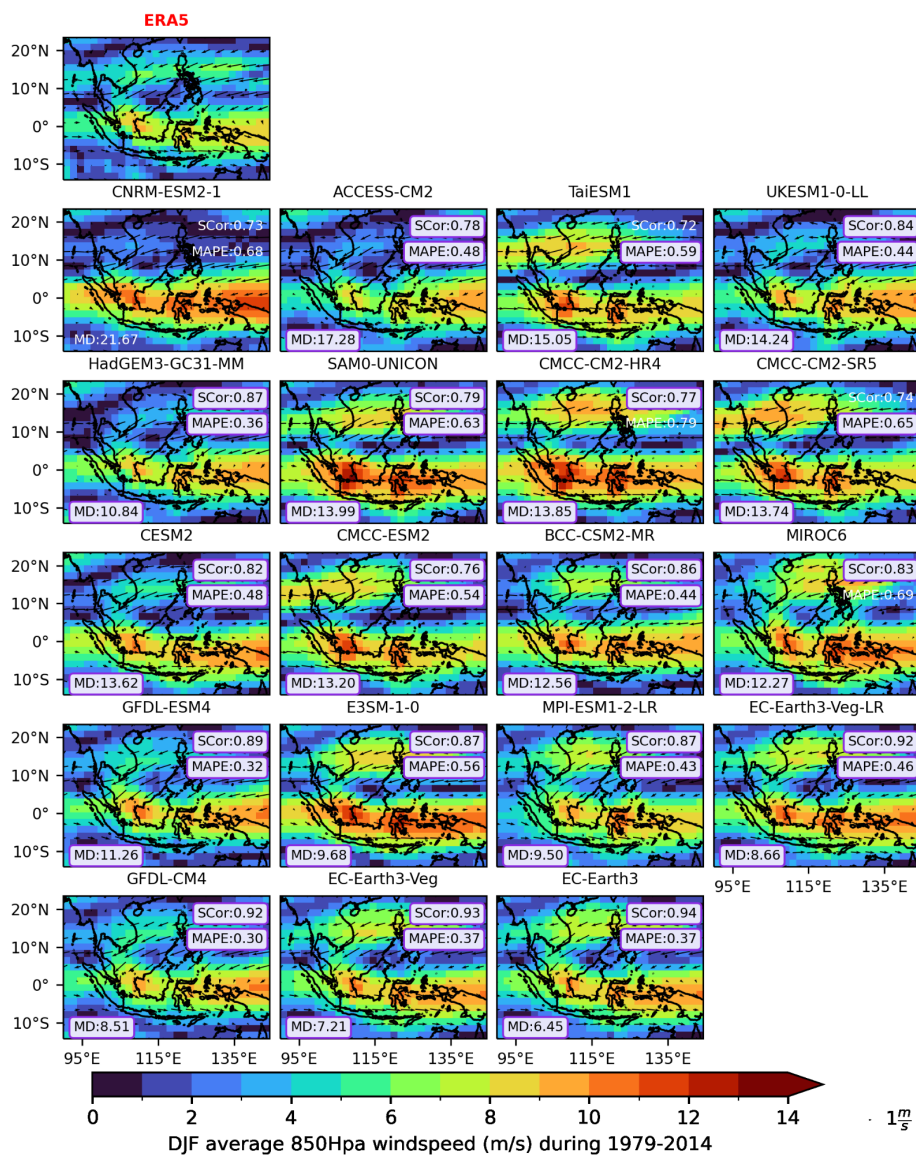
#### 379 **3.2.1. Monsoon wind**

380 We seek to identify models that adequately depict the low-level circulation over SEA during two prominent  
381 seasons: boreal summer (June-September; JJAS) and winter (December-February, DJF), by comparing them to  
382 ERA5 (Fig. 7 and 8 respectively). To measure the agreement between simulated and observed wind patterns in  
383 terms of intensity and direction, we employ three metrics: Scor; MAPE and MD (see section 2.2.3) and we set the  
384 benchmarking threshold for each metric in dealing with limited simulations at this versatility stage. In particular,  
385 we define the threshold for wind intensity as  $\text{MAPE} \leq 0.65$  to seek models that do not overestimate the amplitude  
386 of monsoon wind. In terms of wind structure, we set a stricter benchmarking threshold for Scor as  $\geq 0.70$ , aiming  
387 to retain models that adequately represent the distribution of wind intensity across the whole region. Recognizing  
388 that wind magnitude might be the same at a location, but different directions could substantially impact rainfall  
389 patterns, we consider a threshold for direction MD as  $\leq 20$  degrees. This criterion helps to eliminate models where  
390 high-speed wind direction deviates significantly from observed patterns.



391

392 **Figure 7.** The spatial distribution of the climatology (1979-2014) of low-level wind circulation during the summer (JJAS)  
 393 (vectors) in ERA5 reanalysis (highlighted by red title) and for individual simulations selected using MSM. All analyses are  
 394 considered at the coarsest CMIP6 GCM (i.e., NESM3, ~ 216km). Shading indicates the magnitude of wind (in  $m s^{-1}$ ). The  
 395 mean absolute percentage error (MAPE) and spatial correlation (Scor) calculated against ERA5 are plotted in the upper right  
 396 corners respectively. The mean of difference in wind direction (MD) referenced to ERA5 is shown in the lower left corner.  
 397 Values highlighted in purple-coloured boxes indicate that they meet our defined benchmarking thresholds. Models are ranked  
 398 from highest to lowest values of MD.



399

400 **Figure 8.** Same as Figure 7 but for the boreal winter wind (December-February, DJF)

401 During summer, ERA5 shows westerly winds flowing from the Bay of Bengal into Indochina, then deviating  
 402 northward to the northern Philippines (along 10N). Concurrently, easterly winds from Australia traverse MC and  
 403 Papua (see Fig. 7). Conversely, in winter, the wind patterns are largely reversed (Fig. 8). The easterly winds from  
 404 the north pass through the Philippines, reaching the southern coast of Vietnam and the Malaysian peninsula, while  
 405 westerly winds circulate between the Indonesian islands towards Papua.

406 Overall, the subset of CMIP6 GCMs capture the circulation structure relatively well (Scor ranging from 0.72 to  
 407 0.92 for DJF and from 0.81 to 0.95 for JJAS) but tend to overestimate the wind intensity relative to ERA5,



408 particularly over high-speed wind areas. For example, the westerly component from the Bay of Bengal during  
409 JJAS or the easterly component over MC during DJF is too strong compared to ERA5. These might link with the  
410 wet biases discussed in section 5.1. Interestingly, all MSM-selected models capture the direction of the main  
411 components of JJAS monsoon flow well.

412 Using the definition of benchmark thresholds mentioned above, all models meet our expectations for wind  
413 intensity (MAPE) during the summer season but two fail for the winter season (i.e., MAPE of 0.79 for CMCC-  
414 CM2-HR4 and 0.69 for MIROC6). Interestingly, only one model fails in benchmarking for wind spatial  
415 distribution and direction: CNRM-ESM2-1 (MD is 21.67 during DJF, Fig. 8).

### 416 3.2.3 Rainfall teleconnections with modes of variability

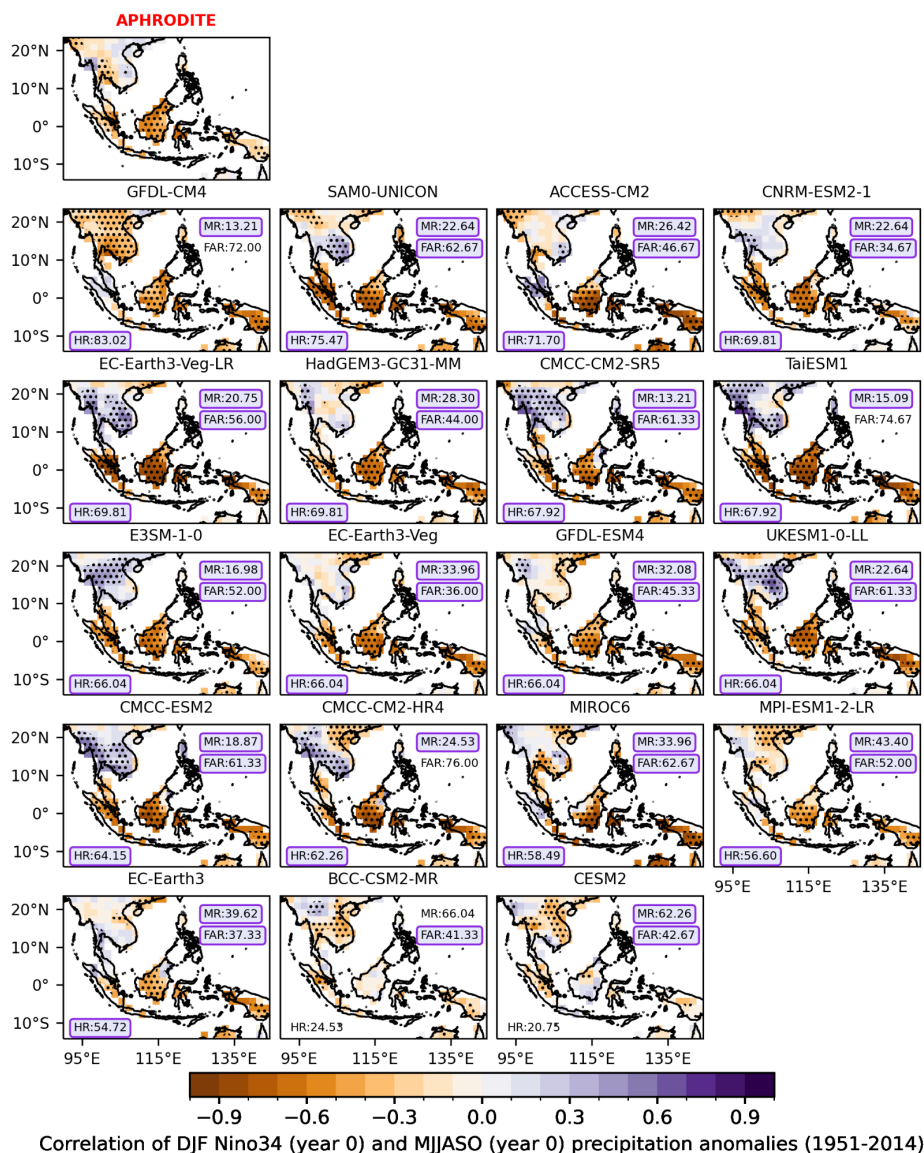
417 The rainfall teleconnection for DJF ENSO is examined for two different seasons: the boreal summer season of the  
418 developing year (MJJASO of year 0) the boreal spring of the following year (MAM of year +1) while the  
419 precipitation-IOD teleconnection is analysed for boreal autumn (SON). To benchmark CMIP6 GCMs, three  
420 considered metrics (HR, MR and FAR, see section 2.2.3) are calculated for each GCM. To benchmark models,  
421 we set benchmarking thresholds  $\geq 50\%$  for HR and  $\leq 65\%$  for MR and FAR, given the limited number of  
422 simulations considered at this stage.

423 The results for observations and CMIP6 GCMs selected from MSMs are shown in Fig. 9-11 respectively. The  
424 observed teleconnections vary widely by region and season. In general, ENSO-induced summer rainfall variability  
425 is dominant over MC (e.g., Sumatra and Java, Fig. 9), while spring variability is dominant over Indochina,  
426 northern Borneo and Philippines (Fig. 10), which agrees with the evolution and seasonal circulation migration  
427 mentioned in previous literature (Juneng and Tangang, 2005; Supari et al., 2018; Wang et al., 2020). On the other  
428 hand, IOD-induced rainfall variability is more pronounced during the SON season over MC (Fig. 11).

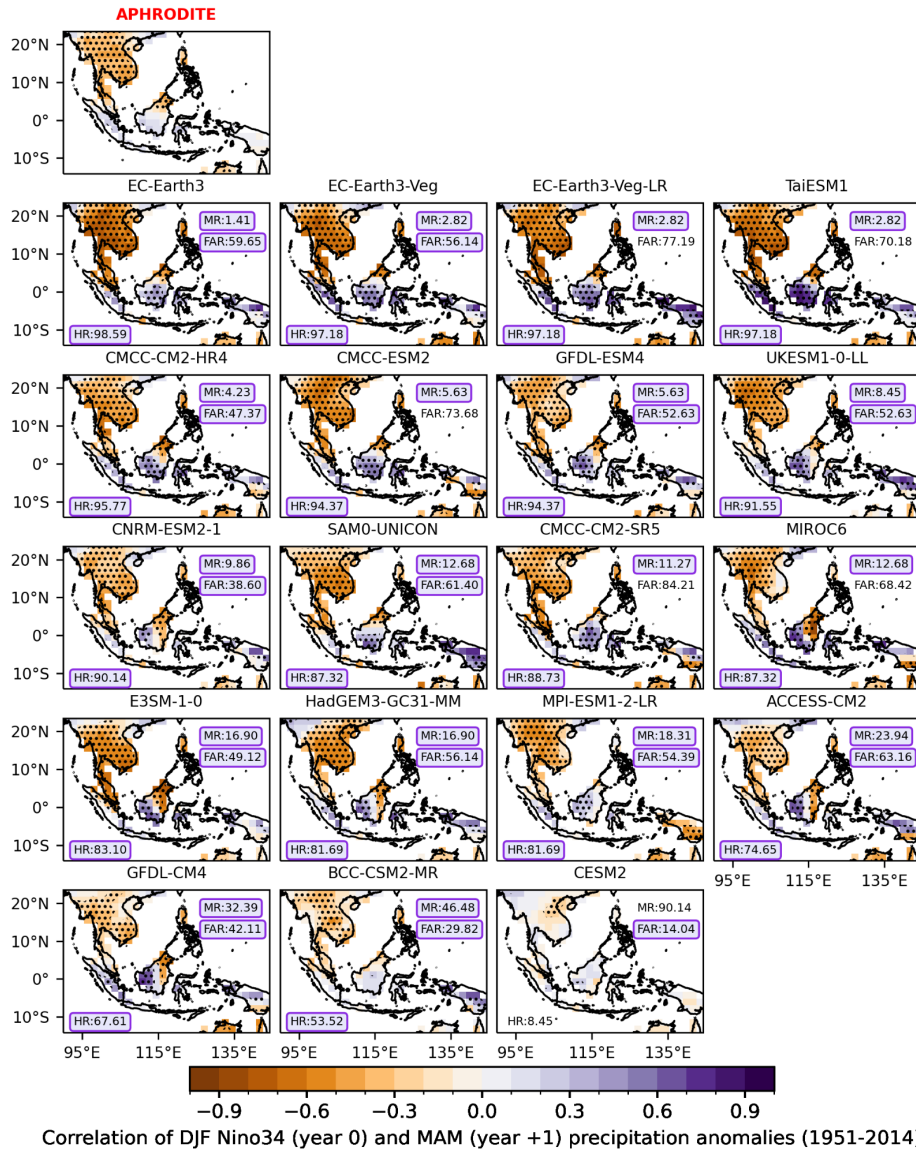
429 CMIP6 GCMs demonstrate reasonable accuracy in simulating the spatial distribution of the ENSO teleconnection,  
430 but tend to overestimate its strength, particularly over regions where observed temporal correlation coefficients  
431 are non-significant. During MJJASO of the developing year, most models successfully reproduce significant  
432 negative signals over MC (e.g., high HR values ranging from 66.04% to 69.81% and low MR values less than  
433 40%). During boreal spring of the following year (MAM of year 1), the ENSO-signals in CMIP6 GCMs match  
434 the observed pattern better than those during MJJASO of the developing year (Fig. 9), particularly over Indochina.  
435 Higher values of HR and lower MRs are found in most CMIP6 GCMs. This is consistent with previous literature  
436 that highlight that GCMs tend to overestimate ENSO variability across much of the equatorial Pacific (Mckenna  
437 et al., 2020) produce a poor representation of the ENSO life cycle (Taschetto et al., 2014; Mckenna et al., 2020)  
438 and interaction between ENSO and IOD (Mckenna et al., 2020; Planton et al., 2021). Note that certain models  
439 consistently perform well across seasons, such as EC-Earth3-Veg, EC-Earth3-CC, GFDL-ESM4 or HadGEM3-  
440 GM31-MM while others, like BCC-CSM2-MR and CESM-2, exhibit less favourable performance in capturing  
441 ENSO teleconnections over the region (Fig. 9 and 10). Eight out of 19 models, including the EC-Earth3 family,  
442 ACCESS-CM2, E3SM1-0, GFDL-ESM4, HadGEM3-GCM31-MM, MPI-ESM1-2-LR, SAM0-UNICON, UK-  
443 ESM1-0-LL meet the ENSO teleconnection benchmark. Among models that did not pass the benchmark, many  
444 indicate an overestimation of observed non-significant ENSO signals (FAR) over the mainland during the  
445 MJJASO of year 0 (e.g., FAR of CMCM-CM2-HR, TaiESM1 and GFDL-CM4 is 76%, 74,67% and 72%



446 respectively) or over MC during MAM of the following year (e.g., FAR of CMCC-CMS-SR5, EC-Earth3-Veg-  
 447 LR and CMCC-ESM2 are 84.21%, 77.19% and 73.69% respectively).



448  
 449 **Figure 9.** Lead correlation coefficients of the boreal summer (May-October, MJJASO year 0) rainfall with the mature phase  
 450 of ENSO (December-January-February, DJF year 0 of Niño3.4 indices) for observations from APHRODITE with HadISST;  
 451 individual CMIP6 GCM models during the period 1951-2014. The stippling indicates the grid points where the correlation  
 452 coefficient is statistically significant at 95% confidence level according to the Student t-test. The Hit Rate (HR), Miss Rate  
 453 (MR) and False Alarm Rate (FAR) calculated against APHRODITE are shown in the bottom left and upper right corners  
 454 respectively. All analyses are considered at the coarsest CMIP6 GCM (i.e., NESM3, ~ 216km). Values highlighted in purple-  
 455 coloured boxes indicate values that meet our defined benchmarking thresholds. Models are ranked from highest to lowest  
 456 values of HR.



457

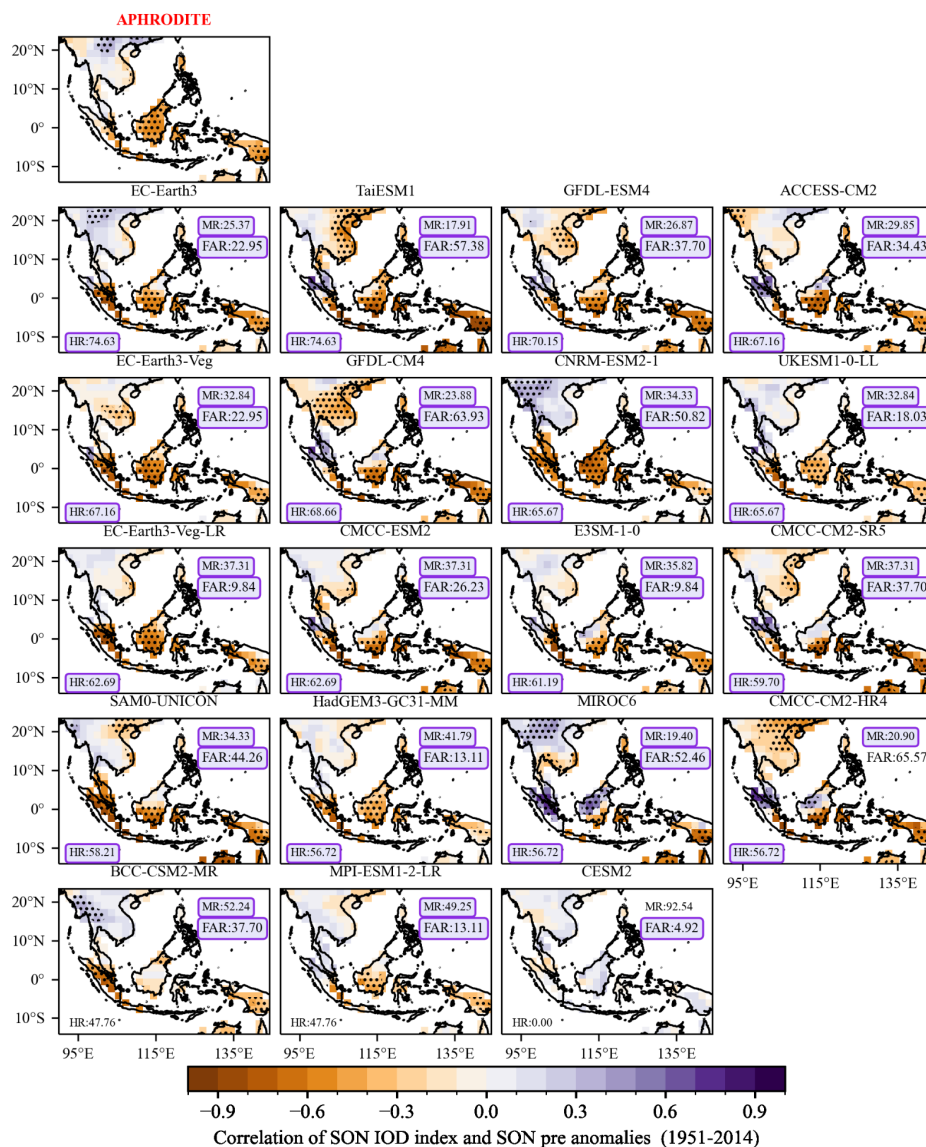
458 **Figure 10.** Similar with Figure 9 but for the lag correlation coefficients the mature phase of ENSO (December-January-  
 459 February, DJF year 0 of Niño3.4 indices) with the boreal spring (March-April-May, MAM year +1) rainfall for (a) observations  
 460 from APHRODITE with HadISST; (b)-(k) individual CMIP6 GCM models during the period 1951-2014. Models are ranked  
 461 from highest to lowest values of HR. All analyses are considered at the coarsest CMIP6 GCM (i.e., NESM3, ~ 216km).

462 Interestingly, the precipitation-IOD teleconnection shows some notable similarities among the 18 CMIP6 GCMs  
 463 considered at the versatility metrics stage. Most models capture the significant negative correlation over Java and  
 464 southern Borneo, resulting in high HR values (ranging from 58.21% to 74.63%). An exception is CESM2, which  
 465 produces non-significant signals over the entire region (Fig. 11). Interestingly, models that demonstrate weak  
 466 performance in simulating ENSO teleconnections (e.g., BCC-CSM2-MR, CESM2 and CNCC-CM2-HR) also





467 struggle to accurately simulate the IOD teleconnection. Using the same threshold definitions as established for  
 468 assessing the ENSO teleconnection, we identify 14 out of 18 models that pass the benchmarking for IOD-  
 469 teleconnection.



470

471 **Figure 11.** Correlation coefficient of the boreal autumn (September-October-November, SON) rainfall with IOD (DMI)  
 472 indices for observations from APHRODITE with HadISST and for individual CMIP6 GCMs during the period 1951-2014.  
 473 The stippling indicates the grid points where the correlation coefficient is statistically significant at 95% confidence level  
 474 according to the Student t-test. The Hit Rate (HR), Miss Rate (MR) and False Alarm Rate (FAR) calculated against  
 475 APHRODITE are plotted in the bottom left and upper right corners respectively. Values highlighted in purple-coloured boxes  
 476 indicate values that meet our defined benchmarking thresholds. Models are ranked from highest to lowest values of HR. All  
 477 analyses are considered at the coarsest CMIP6 GCM (i.e., NESM3, ~ 216km).



478 **Table 4.** Summary model performance against the versatility metrics that focused on precipitation drivers and modes of variability (ENSO and IOD teleconnections). Models fail instantly the  
 479 benchmarks are highlighted in red. All analyses are considered at the coarsest CMIP6 GCM (i.e., NESM3, ~ 216km).  
 480

Simulations	Monsoon circulation						ENSO Teleconnection						IOD teleconnection		Pass/15	
	Score	MIJAS	MAPE	Score	MDJF	HR	MIJASO year 0	FAR	HR	MIR	FAR	HR	MIR	FAR		SON year 0
ACCESS-CM2	+	+	+	+	+	+	+	+	+	+	+	+	+	+	+	15
BCC-CSM2-MR	+	+	+	+	+	+	-	+	+	+	+	+	+	+	+	13
CESM2	+	+	+	+	+	+	+	+	-	+	+	+	+	+	+	10
CMCC-CM2-HR4	+	+	+	-	+	+	-	+	-	+	-	+	-	+	-	11
CMCC-CM2-SR5	+	+	+	+	+	+	+	+	+	+	+	+	+	+	+	14
CMCC-ESM2	+	+	+	+	+	+	+	+	+	+	+	+	+	+	+	14
CNRM-ESM2-1	+	+	+	-	-	-	+	+	+	+	+	+	+	+	+	12
E3SM-1-0	+	+	+	+	+	+	+	+	+	+	+	+	+	+	+	15
EC-Earth3	+	+	+	+	+	+	+	+	+	+	+	+	+	+	+	15
EC-Earth3-Veg	+	+	+	+	+	+	+	+	+	+	+	+	+	+	+	15
EC-Earth3-Veg-LR	+	+	+	+	+	+	+	+	+	+	+	+	+	+	+	14
GFDL-CM4	+	+	+	+	+	+	+	+	-	+	+	+	+	+	+	14
GFDL-ESM4	+	+	+	+	+	+	+	+	+	+	+	+	+	+	+	15
HadGEM3-GC31-MM	+	+	+	+	+	+	+	+	+	+	+	+	+	+	+	15
MIROC6	+	+	+	-	+	+	+	+	+	+	+	-	+	+	+	13
MPI-ESM1-2-LR	+	+	+	+	+	+	+	+	+	+	+	+	-	+	+	14
SAM0-UNICON	+	+	+	+	+	+	+	+	+	+	+	+	+	+	+	15
TaiESM1	+	+	+	+	+	+	+	+	-	+	+	+	-	+	+	13
UKESM1-0-LL	+	+	+	+	+	+	+	+	+	+	+	+	+	+	+	15

481

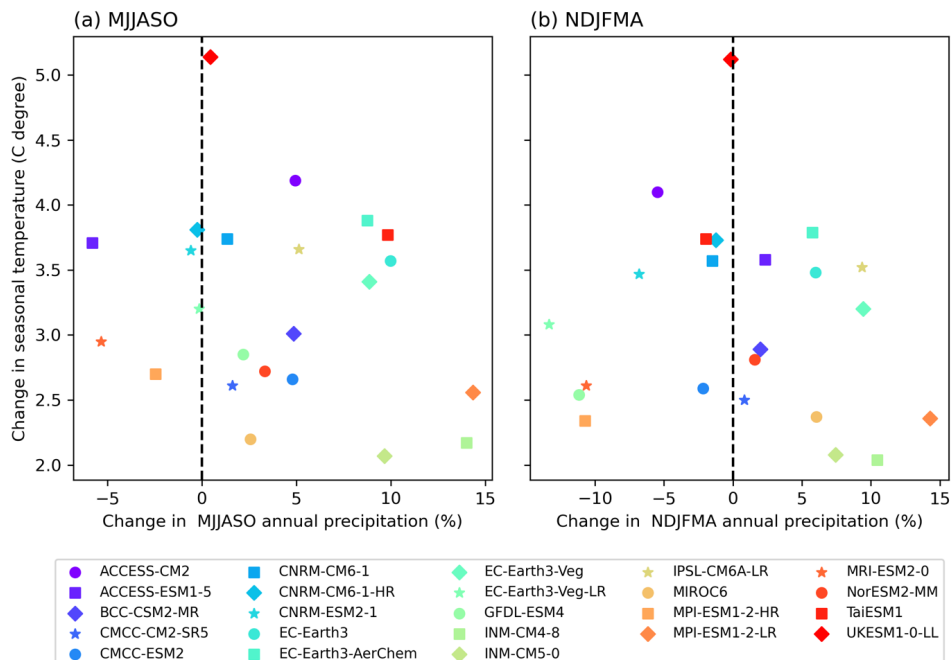


482 Given the large observational uncertainty, particularly in rainfall estimation over the region (Nguyen et al., 2020;  
 483 Nguyen et al., 2022), we apply the BMF using different reference datasets while maintaining a consistent  
 484 benchmarking threshold definition. This evaluation identifies a similar list of models meeting the minimum  
 485 standards of performance (Table s2). However, exceptions are noted, for instance, MPI-ESM1-2-LR fails to meet  
 486 the MSMs when compared with GPDD\_FDD but passes with other references. Similarly, NorESM2-MM exhibits  
 487 varying performance across different observational products. However, even if these two models are included in  
 488 the subsequent selection steps, they fail to meet one or more versatility metrics. For instance, MPI-ESM1-2-LR  
 489 fails the IOD-teleconnection benchmark (Fig. 11 and Table 4) while NorESM2-MM fails on the ENSO-  
 490 teleconnection benchmark; Fig. s5).

491 It is acknowledged that different SST products vary in capturing the teleconnection. Figure s6 indicates the notable  
 492 similarities among SST products in capturing the response of precipitation with modes of variability over SEA  
 493 except for the teleconnection between DJF (year 0) ENSO and MJJASO (year 0) precipitation. However, despite  
 494 the diversity in SST products, the final selection of models passing the BMF remains the same.

495 Table 4 summarises the results of benchmarking 19 CMIP6 GCMs selected from the MSM for the versatility  
 496 metrics. At this point of applying the BMF, we find 8 models (ACCESS-CM2, E3SM1-0, EC-Earth3, EC-Earth3-  
 497 Veg, GFDL-CM4, HadGEM3-GC31-MM, SAM0-UNICON, UKESM1-0-LL) meet our expectations in  
 498 simulating precipitation drivers and teleconnections with modes of variability. This could be due to the fact that  
 499 IOD is an ENSO artefact (Dommenget, 2011).

500 **3.3 Future climate change signals and model dependence**

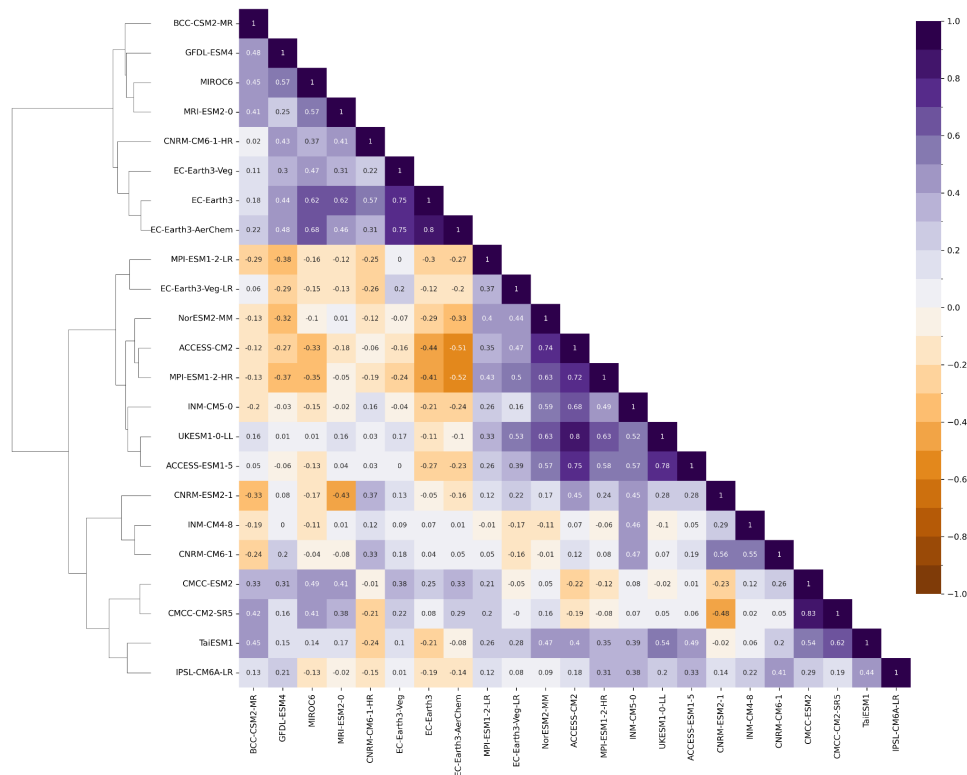


501



502 **Figure 12.** CMIP6 GCM climate change signal (2070-2099 relative to 1961-1990) over mainland Southeast Asia during (a)  
 503 the wet (MJJASO) and (b) the dry (NDJFMA) seasons. The analyses are conducted for the GCMs that simulated at least  
 504 monthly near-surface air temperature (tas) and precipitation (pr) for the SSP-3.70 scenario. Note that some models that did not  
 505 simulate tas or pr for SSP-3.70 (e.g., E3SM1-0, HadGEM3-GCM31-MM, SAM0-UNICON) are not plotted.

506 Climate change signals for CMIP6 GCMs that provide mean temperature and precipitation for the SSP3-7.0  
 507 scenario during two distinct seasons are shown for SEA in Fig. 12. Interestingly, while temperature projections  
 508 show general agreement of an increasing trend (ranging from 2.1°C to 5.1°C), precipitation projections exhibit  
 509 large variation in both direction and magnitude (ranging from -4.3% to 12.9%). Therefore, we cannot see the  
 510 linear relationship between the change in regional total precipitation and temperature. Among the eight models  
 511 that pass our BMF a priori expectations, there are only five models that provide at least data for monthly near-  
 512 surface temperature (tas) and precipitation (pre), and they are distributed across the wide range of temperature  
 513 and precipitation signals over SEA. They include: the wettest models in both seasons with mid-range projected  
 514 temperatures [e.g. for the MJJASO season: EC-Earth3 (10 % and 3.6 °C) and EC-Earth3\_Veg (8.9% and 3.4 °C),  
 515 Fig. 12a]; a model with the largest increase in temperature: UKESM1-0-LL (e.g., 5.1 °C during the MJJASO  
 516 season); a model with larger response in precipitation and lower warming: GFDL-ESM4 (e.g., -11.2 % and 2.5  
 517 °C during the MJJASO season) and a model with a high-range temperature and mid-range precipitation response:  
 518 ACCESS-CM2 (e.g., 4.9% and 4.2 °C during the MJJASO season).



519 **Figure 13.** Dendrogram with hierarchical clustering applied for a matrix of spatial correlation coefficient between CMIP6  
 520 climate models for the long-term changes (2070-2099 SSP3-7.0) relative to 1961-1990 in total precipitation during the wet  
 521 season (MJJASO). The matrix is plotted for GCMs that simulated at least monthly near-surface air temperature (tas)  
 522 and precipitation (pr) for the SSP-3.70 scenario only. Models are clustered with the Ward's linkage criterion.

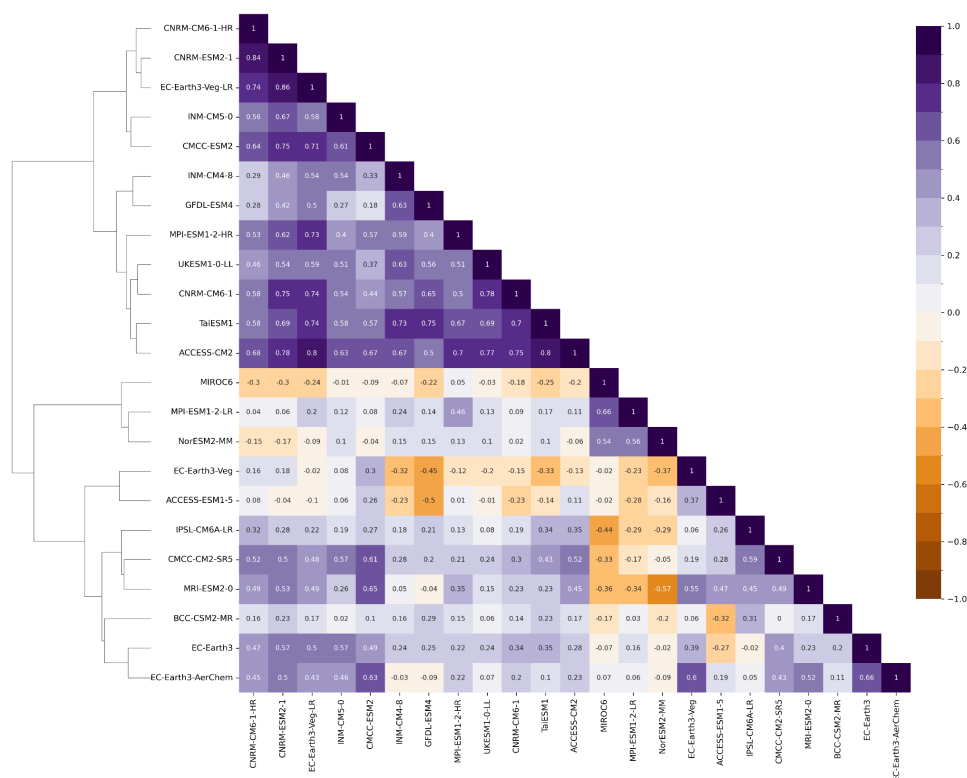


524 The dendrogram and matrix of spatial correlation between CMIP6 GCMs are shown for Southeast Asia for  
525 climatological bias (Fig. s7-8) and long-term changes (Fig. 13-14) in total precipitation. As before we focus on  
526 the wet (MJJASO) and dry (NDJFMA) seasons. Historical correlations highlight notable similarities between  
527 models in historical bias maps (mostly significant and greater than 0.5) except UK-ESM1-0-LL which shows  
528 poorer relationships with other models (e.g., correlation coefficients with other models are less than 0.5) (Fig s7-  
529 8). However, there is higher independence in projection maps compared with that in historical maps. This can be  
530 explained by the fact that historical simulations were constrained by observational data (e.g., observed SSTs).  
531 Future simulations on the other hand, are free running and dependent on the model setup, leading to different  
532 ranges of regional climate response across GCMs.

533 Clustering analysis indicates three main spatial change clusters for the MJJASO season, as shown in the MJJASO  
534 dendrogram (Fig. 13). This indicates similarities in the spatial pattern of the climate change response maps (e.g.,  
535 correlations greater than 0.5) not only among models from the same families [e.g., among the MetOffice GCM-  
536 based family (i.e., UKESM1-0-LL, ACCESS's family)] and in model families that share the same model  
537 components (e.g., UK-ESM1-0-LL and EC-Earth3 families share the same ocean model of NEMO3.6; Table 1)  
538 but also in less obvious families like CNRM and INM families or EC-Earth-based and GFDL-based simulations.  
539 An exception is EC-Earth-Veg-LR which appears in different main clusters compared with other EC-Earth-based  
540 simulations. As indicated in the MJJASO dendrogram, the BMF-passing models that have data available for  
541 dynamical downscaling are in two main clusters including: EC-Earth3/ EC-Earth-veg/ GFDL-ESM4 and  
542 UKESM1-0-LL/ ACCESS-CM2.

543 Figure 14 indicates two main spatial change clusters in the dry season. Interestingly, some models from the same  
544 family (e.g., EC-Earth3 and EC-Earth-Veg) still belong to the same main cluster but span different branches of  
545 the dendrogram. This might be related to the different role of internal variability in determining the level of  
546 uncertainty for precipitation during different seasons and needs further investigation. Interestingly, among models  
547 that pass the BMF, EC-Earth3 and EC-Earth-veg appear on a main cluster while UKESM1-0-LL, ACCESS-CM2  
548 and GFDL-ESM4 are in the other main cluster for the NDJFMA dendrogram. This highlights the dependence of  
549 clustering analysis on the season.

550



551

552 **Figure 14.** Similar to figure 13 but for the dry season (November – April, NDJFMA)

553 In general, based on our evaluation of model performance, model dependence and future climate change spread,  
 554 we identify two independent groups of models to use for dynamical downscaling over SEA, that is, EC-Earth3/  
 555 EC-Earth-Veg, ACCESS-CM2/UKESM1-0-LL. Given the inconsistency of classification of GFDL-ESM4 during  
 556 different seasons and metrics, it is suggested to consider GFDL-ESM4 with caution.

557 **4 Discussion**

558 Our results somewhat differ from traditional model evaluation studies like Desmet and Ngo-Duc (2022), which  
 559 ranks models by evaluation metrics and identifies a list of the best models including EC-Earth3, EC-Earth3-Veg,  
 560 CNRM-CM6-1-HR, FGOALS-f3-L, HadGEM3-GC31-MM, GISS-E2-1-G, GFDL-ESM4, CIESM-WACCM  
 561 and FIO-ESM-2-0. First, rather than ranking models, our aim is to retain models that meet our predefined  
 562 expectations (e.g., benchmarking thresholds). Second, the list of examined models is different since we especially  
 563 focus on models with a resolution greater than 2 degrees to avoid the impacts of coarser resolutions in GCMs on  
 564 dynamical downscaling. Furthermore, while Desmet and Ngo-Duc (2022) combine model performance in  
 565 simulating surface climates (e.g., precipitation, near-surface temperature) and climate processes (e.g., low-level  
 566 atmospheric circulation), our focus is solely on precipitation, its drivers and teleconnections with modes of  
 567 variability.



568 We acknowledge that the list of models passing the BMF might change, depending on how the benchmarking  
569 thresholds are defined. Ispording et al. (2024) notes that the definition of the benchmarking thresholds for the  
570 MSMs and versatility metrics can be subjective, and they should be chosen to fit the purpose of the study while  
571 incorporating strong scientific reasoning. The strategy employed here involves defining the benchmarking  
572 thresholds based on our knowledge of observational uncertainty over the region. In addition, we aim to give each  
573 model the ‘benefit of doubt’, thus retaining a broad range of plausible future climate change responses. In  
574 particular, in the initial step of the BMF framework, we are generous in defining the benchmark threshold for the  
575 wet season given the lower model performance compared with the dry season. This approach results in 19 out of  
576 32 models passing the MSMs. Subsequently we employ versatility metrics to cover a more process-based  
577 assessment. Given previous studies have highlighted the overestimation of GCMs in simulating precipitation  
578 drivers and its teleconnections and limited possible simulations at this stage, we also set relaxed thresholds for  
579 various metrics to maximize the number of models passing the BMF. We feel this is a pragmatic approach to  
580 retain a reasonable sample size and explore plausible futures. However, we acknowledge that dynamical  
581 downscaling experiments often require significant computing resources and only a small subset of GCMs should  
582 be pre-selected. Therefore, we narrow down our selection of 8 GCMs for further assessment using metrics related  
583 to model dependency and future climate change spread.

584 Previous studies suggest the potential impact of smoothing the extreme values when interpolating to coarser  
585 resolutions, which might affect the skill score metrics used to measure percentage errors in a simulation relative  
586 to a reference (i.e., MAPE). Although we observe a higher number of failed models for the same skill when  
587 conducting the BMF at the GCM original resolutions (Table s4), we identify a similar subset of models meeting  
588 all minimum performance requirements (Table s4). This suggests that the coarser resolution of ~210 km used for  
589 benchmarking is not the main reason behind the results of quantifying model skill used in this study. This is in  
590 line with Nguyen et al. (2022), where they demonstrate that model components (e.g., configurations in different  
591 schemes) are the main reason behind the model biases rather than model resolution.

592 The relationship between model structures and model biases is investigated in the model dependency section using  
593 cluster analysis. We acknowledge that grouping of models might changes for not only for considered periods and  
594 seasons (as discussed in section 3.3) but also for considered metrics. Interestingly, using mean percentage changes  
595 as distance measure between models, we identify similar main clusters of EC-Earth3/ EC-Earth-Veg and  
596 ACCESS-CM2/ UKESM1-0-LL among models that passing the BMF (Fig. s9-s10). This subset of models is  
597 suitable for dynamical downscaling over Southeast Asia.

598 The customized BMF implemented in this study offers a consistent framework for model evaluation across the  
599 whole CORDEX-SEA domain. The framework can be further developed and applied extensively to sub-regions  
600 of interest, in particular within the upcoming Climatic hazard Assessment to enhance Resilience against climate  
601 Extremes for Southeast Asian megacities (CARE for SEA megacities) Project of CORDEX-SEA. In this project,  
602 each mega city can identify their climate priority and the associated metrics for selecting a fit-for-purpose subset  
603 of models. This framework could also be implemented in impact-related projections over SEA, for particular  
604 sectors: agriculture, forestry, water etc. for credible future projections.



605 **5 Conclusion**

606 In this paper, we apply the insight gained from the CMIP6 selection process for dynamical downscaling across  
607 various CORDEX-domains to Southeast Asia by encompassing several critical factors: model performance, model  
608 independence, data availability and the spread of future climate change projections.

609 Rather than exhaustively evaluating all performance aspects of the models in simulating the Southeast Asian  
610 climate, our focus is on selecting models that simulate precipitation well, including its drivers and teleconnections  
611 given the high uncertainty in rainfall projections over the region. In addition, we apply a novel standardised  
612 benchmarking framework – a new approach in identifying a subset of fit-for-purpose models that align with a  
613 user’s a priori performance expectations. This framework has two stages of assessment: statistical-based metrics  
614 and process/regime-based metrics, conducted for both wet (MJJASO) and dry (NDJFMA) seasons.

615 From the first step we identify 19 GCMs that meet our minimum criteria for simulating the fundamental  
616 characteristics (e.g., bias, spatial distribution, seasonality, and trends) of seasonal rainfall. GCMs generally exhibit  
617 wet biases, particularly over the complex terrain of the Maritime Continent. These models then undergo a second  
618 evaluation, focusing on their ability to simulate climate processes and teleconnections with modes of variability.  
619 While these models consistently capture atmospheric circulation and teleconnections with modes of variability  
620 over the region, they exhibit a tendency to overestimate their strength. Ultimately, our framework narrows down  
621 the selection to eight GCMs that meet our model performance expectations in simulating fundamental  
622 characteristics of precipitation, key drivers, and teleconnections over Southeast Asia. There are obvious high-  
623 performing GCMs from allied modelling groups, highlighting the dependency of the subset of models identified  
624 from the framework. Consequently, additional tests on model independence, data availability for the SSP 3-7.0,  
625 and the spread of future climate change are conducted. These tests lead to the identification of two independent  
626 groups of models (e.g., EC-Earth3-Veg/EC-Earth3 and ACCESS-CM2/UKESM1-0-LL) that align with our  
627 a priori expectations for dynamical downscaling over CORDEX-SEA. It is recommended that only one model from  
628 each group be chosen to avoid models that are too closely related.

629 **Code availability**

630 Codes for benchmarking the CMIP6 GCMs performance (Isphording, 2024) are available from  
631 <https://doi.org/10.5281/zenodo.8365065>

632 **Data availability**

633 Data used in this study is available through:  
634 CMIP6 GCMS at the Earth System Grid Federation (ESGF):  
635 <https://esgf.nci.org.au/projects/esgf-nci/>.  
636 ERA5 (Hersbach et al. 2020): <https://doi.org/10.24381/cds.bd0915c6>.  
637 OISST version 2.1 (Huang et al. 2021):  
638 <https://www.psl.noaa.gov/data/gridded/data.noaa.oisst.v2.highres.html>.  
639 ERSST version 5 (Huang et al. 2017):  
640 <https://www.ncei.noaa.gov/pub/data/cmb/ersst/v5/netcdf/>.





641 APHRODITE version V1101R1 and V1101 XR (Yatagai et al., 2012):

642 <https://www.chikyu.ac.jp/precip/english/index.html>.

643 **Author contributions**

644 RNI built the BMF used in this research. PLN applied and developed the BMF for the region of interest, performed  
645 the analysis and prepared the original manuscript. LVA, MJT, SCHN and JLM supervised the research, reviewed  
646 and edited the manuscript.

647 **Declaration of Competing Interests**

648 The authors declare that they have no known competing financial interests or personal relationships that could  
649 have appeared to influence.

650 **Acknowledgements**

651 This work was supported by the Australian Research Council (ARC) Grant FT210100459. LVA and RNI are also  
652 supported by ARC grant CE17010023. RNI is also supported by a Scientia PhD scholarship from UNSW. The  
653 research was undertaken with the assistance of resources and services from the National Computational  
654 Infrastructure (NCI), which is supported by the Australian Government. The codes and graphics visualization for  
655 the assessment of CMIP6 GCMs based on the benchmarking framework suggested in Ispording et al. (2024) and  
656 Ispording (2024).



## References

- 660 Abramowitz, G.: Towards a benchmark for land surface models, *Geophysical Research Letters*, 32, <https://doi.org/10.1029/2005GL024419>, 2005.
- Abramowitz, G.: Towards a public, standardized, diagnostic benchmarking system for land surface models, *Geosci. Model Dev.*, 5, 819-827, 10.5194/gmd-5-819-2012, 2012.
- Alexander, L. V., Bador, M., Roca, R., Contractor, S., Donat, M. G., and Nguyen, P. L.: Intercomparison of annual precipitation indices and extremes over global land areas from in situ, space-based and reanalysis products, *Environmental Research Letters*, 665 15, <https://doi.org/10.1088/1748-9326/ab79e2>, 2020.
- Allan, R., Chambers, D., Drosowsky, W., Hendon, H., Latif, M., Nicholls, N., Smith, I., Stone, R., and Tourre, Y.: Is there an Indian Ocean dipole and is it independent of the El Niño-Southern Oscillation, *CLIVAR exchanges*, 21, 18-22, 2001.
- Amirudin, A. A., Salimun, E., Tangang, F., Juneng, L., and Zuhairi, M.: Differential influences of teleconnections from the Indian and Pacific Oceans on rainfall variability in Southeast Asia, *Atmosphere*, 11, 886, 2020.
- 670 Andrews, M. B., Ridley, J. K., Wood, R. A., Andrews, T., Blockley, E. W., Booth, B., Burke, E., Dittus, A. J., Florek, P., Gray, L. J., Haddad, S., Hardiman, S. C., Hermanson, L., Hodson, D., Hogan, E., Jones, G. S., Knight, J. R., Kuhlbrodt, T., Misios, S., Mizielinski, M. S., Ringer, M. A., Robson, J., and Sutton, R. T.: Historical Simulations With HadGEM3-GC3.1 for CMIP6, *Journal of Advances in Modeling Earth Systems*, 12, e2019MS001995, <https://doi.org/10.1029/2019MS001995>, 2020.
- 675 Baquero-Bernal, A., Latif, M., and Legutke, S.: On dipolelike variability of sea surface temperature in the tropical Indian Ocean, *Journal of Climate*, 15, 1358-1368, 2002.
- Best, M. J.: The plumbing of land surface models: benchmarking model performance, *J. Hydrometeor.*, 16, 1425, <https://doi.org/10.1175/JHM-D-14-0158.1>, 2015.
- 680 Bi, D., Dix, M., Marsland, S., O'Farrell, S., Sullivan, A., Bodman, R., Law, R., Harman, I., Srbinovsky, J., Rashid, H. A., Dobrohotoff, P., Mackallah, C., Yan, H., Hirst, A., Savita, A., Dias, F. B., Woodhouse, M., Fiedler, R., and Heerdegen, A.: Configuration and spin-up of ACCESS-CM2, the new generation Australian Community Climate and Earth System Simulator Coupled Model, *Journal of Southern Hemisphere Earth Systems Science*, 70, 225-251, <https://doi.org/10.1071/ES19040>, 2020.
- Birch, C., Webster, S., Peatman, S., Parker, D., Matthews, A., Li, Y., and Hassim, M.: Scale interactions between the MJO and the western Maritime Continent, *Journal of Climate*, 29, 2471-2492, <https://doi.org/10.1175/JCLI-D-15-0557.1>, 2016.
- 685 Boé, J.: Interdependency in Multimodel Climate Projections: Component Replication and Result Similarity, *Geophysical Research Letters*, 45, 2771-2779, <https://doi.org/10.1002/2017GL076829>, 2018.
- Boucher, O., Servonnat, J., Albright, A. L., Aumont, O., Balkanski, Y., Bastrikov, V., Bekki, S., Bonnet, R., Bony, S., Bopp, L., Braconnot, P., Brockmann, P., Cadule, P., Caubel, A., Cheruy, F., Codron, F., Cozic, A., Cugnet, D., D'Andrea, F., Davini, P., de Lavergne, C., Denvil, S., Deshayes, J., Devillers, M., Ducharme, A., Dufresne, J.-L., Dupont, E., Éthé, C., Fairhead, L., 690 Falletti, L., Flavoni, S., Foujols, M.-A., Gardoll, S., Gastineau, G., Ghattas, J., Grandpeix, J.-Y., Guenet, B., Guez, L., E., Guilyardi, E., Guimberteau, M., Hauglustaine, D., Hourdin, F., Idelkadi, A., Joussaume, S., Kageyama, M., Khodri, M.,



- Krinner, G., Lebas, N., Levavasseur, G., Lévy, C., Li, L., Lott, F., Lurton, T., Luyssaert, S., Madec, G., Madeleine, J.-B., Maignan, F., Marchand, M., Marti, O., Mellul, L., Meurdesoif, Y., Mignot, J., Musat, I., Ottlé, C., Peylin, P., Planton, Y., Polcher, J., Rio, C., Rochetin, N., Rousset, C., Sepulchre, P., Sima, A., Swingedouw, D., Thiéblemont, R., Traore, A. K., Vancoppenolle, M., Vial, J., Vialard, J., Viovy, N., and Vuichard, N.: Presentation and Evaluation of the IPSL-CM6A-LR Climate Model, *Journal of Advances in Modeling Earth Systems*, 12, e2019MS002010, <https://doi.org/10.1029/2019MS002010>, 2020.
- 695 Braganza, K., Karoly, D., Hirst, A., Mann, M., Stott, P., Stouffer, R., and Tett, S.: Simple indices of global climate variability and change: Part I – variability and correlation structure, *Climate Dynamics*, 20, 491-502, 10.1007/s00382-002-0286-0, 2003.
- 700 Brands, S.: Common Error Patterns in the Regional Atmospheric Circulation Simulated by the CMIP Multi-Model Ensemble, *Geophysical Research Letters*, 49, e2022GL101446, <https://doi.org/10.1029/2022GL101446>, 2022.
- Brunner, L., Pendergrass, A. G., Lehner, F., Merrifield, A. L., Lorenz, R., and Knutti, R.: Reduced global warming from CMIP6 projections when weighting models by performance and independence, *Earth Syst. Dynam.*, 11, 995-1012, 10.5194/esd-11-995-2020, 2020.
- 705 Cao, J., Wang, B., Yang, Y. M., Ma, L., Li, J., Sun, B., Bao, Y., He, J., Zhou, X., and Wu, L.: The NUIST Earth System Model (NESM) version 3: description and preliminary evaluation, *Geosci. Model Dev.*, 11, 2975-2993, 10.5194/gmd-11-2975-2018, 2018.
- Chang, C. P., Wang, Z., McBride, J., and Liu, C.-H.: Annual Cycle of Southeast Asia -- Maritime Continent Rainfall and the Asymmetric Monsoon Transition, *Journal of Climate* 18, 287-301, <https://doi.org/10.1175/JCLI-3257.1>, 2005.
- 710 Chen, C., Sahany, S., Moise, A. F., Chua, X. R., Hassim, M. E., Lim, G., and Prasanna, V.: ENSO–Rainfall Teleconnection over the Maritime Continent Enhances and Shifts Eastward under Warming, *Journal of Climate*, 36, 4635-4663, <https://doi.org/10.1175/JCLI-D-23-0036.1>, 2023.
- Chen, T.-C., Tsay, J.-D., Yen, M.-C., and Matsumoto, J.: Interannual variation of the winter rainfall in Malaysia caused by the activity of rain-producing disturbances, *Journal of climate*, 26, 4630-4648, <https://doi.org/10.1175/JCLI-D-12-00367.1>, 2013.
- 715 Cherchi, A., Fogli, P. G., Lovato, T., Peano, D., Iovino, D., Gualdi, S., Masina, S., Scoccimarro, E., Materia, S., Bellucci, A., and Navarra, A.: Global Mean Climate and Main Patterns of Variability in the CMCC-CM2 Coupled Model, *Journal of Advances in Modeling Earth Systems*, 11, 185-209, <https://doi.org/10.1029/2018MS001369>, 2019.
- Contractor, S., Donat, M. G., and Alexander, L. V.: Intensification of the daily wet day rainfall distribution across Australia, *Geophysical Research Letters*, 45, 8568-8576, 2018.
- 720 Contractor, S., Donat, M. G., Alexander, L. V., Ziese, M., Meyer-Christoffer, A., Schneider, U., Rustemeier, E., Becker, A., Durre, I., and Vose, R. S.: Rainfall Estimates on a Gridded Network (REGEN) – a global land-based gridded dataset of daily precipitation from 1950 to 2016, *Hydrol. Earth Syst. Sci.*, 24, 919-943, <https://doi.org/10.5194/hess-24-919-2020>, 2020.
- CORDEX: CORDEX experiment design for dynamical downscaling of CMIP6, [https://cordex.org/wp-content/uploads/2021/05/CORDEX-CMIP6\\_exp\\_design\\_RCM.pdf](https://cordex.org/wp-content/uploads/2021/05/CORDEX-CMIP6_exp_design_RCM.pdf), 2021.
- 725 D'Arrigo, R. and Wilson, R.: El Nino and Indian Ocean influences on Indonesian drought: implications for forecasting rainfall and crop productivity, *International Journal of Climatology: A Journal of the Royal Meteorological Society*, 28, 611-616, 2008.



- Danabasoglu, G., Lamarque, J.-F., Bacmeister, J., Bailey, D. A., DuVivier, A. K., Edwards, J., Emmons, L. K., Fasullo, J., Garcia, R., Gettelman, A., Hannay, C., Holland, M. M., Large, W. G., Lauritzen, P. H., Lawrence, D. M., Lenaerts, J. T. M., Lindsay, K., Lipscomb, W. H., Mills, M. J., Neale, R., Oleson, K. W., Otto-Bliesner, B., Phillips, A. S., Sacks, W., Tilmes, S., van Kampenhout, L., Vertenstein, M., Bertini, A., Dennis, J., Deser, C., Fischer, C., Fox-Kemper, B., Kay, J. E., Kinnison, D., Kushner, P. J., Larson, V. E., Long, M. C., Mickelson, S., Moore, J. K., Nienhouse, E., Polvani, L., Rasch, P. J., and Strand, W. G.: The Community Earth System Model Version 2 (CESM2), *Journal of Advances in Modeling Earth Systems*, 12, e2019MS001916, <https://doi.org/10.1029/2019MS001916>, 2020.
- 730 Deng, X., Perkins-Kirkpatrick, S. E., Lewis, S. C., and Ritchie, E. A.: Evaluation of Extreme Temperatures Over Australia in the Historical Simulations of CMIP5 and CMIP6 Models, *Earth's Future*, 9, e2020EF001902, <https://doi.org/10.1029/2020EF001902>, 2021.
- Desmet, Q. and Ngo-Duc, T.: A novel method for ranking CMIP6 global climate models over the southeast Asian region, *International Journal of Climatology*, 42, 97-117, <https://doi.org/10.1002/joc.7234>, 2022.
- 740 Di Virgilio, G., Ji, F., Tam, E., Nishant, N., Evans, J. P., Thomas, C., Riley, M. L., Beyer, K., Grose, M. R., Narsey, S., and Delage, F.: Selecting CMIP6 GCMs for CORDEX Dynamical Downscaling: Model Performance, Independence, and Climate Change Signals, *Earth's Future*, 10, e2021EF002625, <https://doi.org/10.1029/2021EF002625>, 2022.
- Diaconescu, E. P. and Laprise, R.: Can added value be expected in RCM-simulated large scales?, *Climate Dynamics*, 41, 1769-1800, <https://doi.org/10.1007/s00382-012-1649-9>, 2013.
- 745 Díaz, L. B., Saurral, R. I., and Vera, C. S.: Assessment of South America summer rainfall climatology and trends in a set of global climate models large ensembles, *International Journal of Climatology*, 41, E59-E77, <https://doi.org/10.1002/joc.6643>, 2021.
- DOE, U. S.: Benchmarking Simulated Precipitation in Earth System Models Workshop Report, DOE/SC-0203, U.S. Department of Energy Office of Science, Biological and Environmental Research (BER) Program, Germantown, Maryland, USA, 2020.
- 750 Dommenges, D.: An objective analysis of the observed spatial structure of the tropical Indian Ocean SST variability, *Climate Dynamics*, 36, 2129-2145, [10.1007/s00382-010-0787-1](https://doi.org/10.1007/s00382-010-0787-1), 2011.
- Donat, M. G., Delgado-Torres, C., De Luca, P., Mahmood, R., Ortega, P., and Doblas-Reyes, F. J.: How Credibly Do CMIP6 Simulations Capture Historical Mean and Extreme Precipitation Changes?, *Geophysical Research Letters*, 50, e2022GL102466, <https://doi.org/10.1029/2022GL102466>, 2023.
- 755 Dong, T. and Dong, W.: Evaluation of extreme precipitation over Asia in CMIP6 models, *Climate Dynamics*, 57, 1751-1769, [10.1007/s00382-021-05773-1](https://doi.org/10.1007/s00382-021-05773-1), 2021.
- Döscher, R., Acosta, M., Alessandri, A., Anthoni, P., Arsouze, T., Bergman, T., Bernardello, R., Boussetta, S., Caron, L. P., Carver, G., Castrillo, M., Catalano, F., Cvijanovic, I., Davini, P., Dekker, E., Doblas-Reyes, F. J., Docquier, D., Echevarria, P., Fladrich, U., Fuentes-Franco, R., Gröger, M., v. Hardenberg, J., Hieronymus, J., Karami, M. P., Keskinen, J. P., Koenigk, T., Makkonen, R., Massonnet, F., Ménégou, M., Miller, P. A., Moreno-Chamarro, E., Nieradzki, L., van Noije, T., Nolan, P., O'Donnell, D., Ollinaho, P., van den Oord, G., Ortega, P., Prims, O. T., Ramos, A., Reerink, T., Rousset, C., Ruprich-Robert, Y., Le Sager, P., Schmith, T., Schrödner, R., Serva, F., Sicardi, V., Sloth Madsen, M., Smith, B., Tian, T., Tourigny, E., Uotila, P., Vancoppenolle, M., Wang, S., Wårlind, D., Willén, U., Wyser, K., Yang, S., Yepes-Arbós, X., and Zhang, Q.: The EC-Earth3 Earth system model for the Coupled Model Intercomparison Project 6, *Geosci. Model Dev.*, 15, 2973-3020, [10.5194/gmd-15-2973-2022](https://doi.org/10.5194/gmd-15-2973-2022), 2022.
- 765



- 770 Douville, H., Raghavan, K., Renwick, J., Allan, R. P., Arias, P. A., Barlow, M., Cerezo-Mota, R., Cherchi, A., Gan, T. Y., Gergis, J., Jiang, D., Khan, A., Pokam Mba, W., Rosenfeld, D., Tierney, J., and Zolina, O.: Water Cycle Changes, in: Climate Change 2021: The Physical Science Basis. Contribution of Working Group I to the Sixth Assessment Report of the Intergovernmental Panel on Climate Change, edited by: Masson-Delmotte, V., Zhai, P., Pirani, A., Connors, S. L., Péan, C., Berger, S., Caud, N., Chen, Y., Goldfarb, L., Gomis, M. I., Huang, M., Leitzell, K., Lonnoy, E., Matthews, J. B. R., Maycock, T. K., Waterfield, T., Yelekçi, O., Yu, R., and Zhou, B., Cambridge University Press, Cambridge, United Kingdom and New York, NY, USA, 1055–1210, 10.1017/9781009157896.010, 2021.
- 775 Dunne, J. P., Horowitz, L. W., Adcroft, A. J., Ginoux, P., Held, I. M., John, J. G., Krasting, J. P., Malyshev, S., Naik, V., Paulot, F., Shevliakova, E., Stock, C. A., Zadeh, N., Balaji, V., Blanton, C., Dunne, K. A., Dupuis, C., Durachta, J., Dussin, R., Gauthier, P. P. G., Griffies, S. M., Guo, H., Hallberg, R. W., Harrison, M., He, J., Hurlin, W., McHugh, C., Menzel, R., Milly, P. C. D., Nikonov, S., Paynter, D. J., Ploshay, J., Radhakrishnan, A., Rand, K., Reichl, B. G., Robinson, T., Schwarzkopf, D. M., Sentman, L. T., Underwood, S., Vahlenkamp, H., Winton, M., Wittenberg, A. T., Wyman, B., Zeng, Y., and Zhao, M.: The GFDL Earth System Model Version 4.1 (GFDL-ESM 4.1): Overall Coupled Model Description and Simulation Characteristics, *Journal of Advances in Modeling Earth Systems*, 12, e2019MS002015, <https://doi.org/10.1029/2019MS002015>, 2020.
- 780 Evans, J., Virgilio, G., Hirsch, A., Hoffmann, P., Remedio, A. R., Ji, F., Rockel, B., and Coppola, E.: The CORDEX-Australasia ensemble: evaluation and future projections, *Climate Dynamics*, 57, 10.1007/s00382-020-05459-0, 2021.
- 785 Funk, C., Peterson, P., Landsfeld, M., Pedreros, D., Verdin, J., Shukla, S., Husak, G., Rowland, J., Harrison, L., Hoell, A., and Michaelsen, J.: The climate hazards infrared precipitation with stations—a new environmental record for monitoring extremes, *Scientific Data*, 2, 150066, <https://doi.org/10.1038/sdata.2015.66>, 2015.
- Gibson, P. B., Perkins-Kirkpatrick, S. E., Alexander, L. V., and Fischer, E. M.: Comparing Australian heat waves in the CMIP5 models through cluster analysis, *Journal of Geophysical Research: Atmospheres*, 122, 3266–3281, <https://doi.org/10.1002/2016JD025878>, 2017.
- 790 Gibson, P. B., Rampal, N., Dean, S. M., and Morgenstern, O.: Storylines for Future Projections of Precipitation Over New Zealand in CMIP6 Models, *Journal of Geophysical Research: Atmospheres*, 129, e2023JD039664, <https://doi.org/10.1029/2023JD039664>, 2024.
- Giorgi, F. and Gao, X.: Regional earth system modeling: review and future directions, *Atmospheric and Oceanic Science Letters*, 11, 1–9, <https://doi.org/10.1080/16742834.2018.1452520>, 2018.
- 795 Giorgi, F., Jones, C., and Asrar, G.: Addressing climate information needs at the regional level: The CORDEX framework, *WMO Bull*, 53, 2008.
- Giorgi, F., Coppola, E., Teichmann, C., and Jacob, D.: Editorial for the CORDEX-CORE Experiment I Special Issue, *Climate Dynamics*, 57, 1265–1268, <https://doi.org/10.1007/s00382-021-05902-w>, 2021.
- 800 Grose, M. R., Narsey, S., Trancoso, R., Mackallah, C., Delage, F., Dowdy, A., Di Virgilio, G., Watterson, I., Dobrohotoff, P., Rashid, H. A., Rauniyar, S., Henley, B., Thatcher, M., Syktus, J., Abramowitz, G., Evans, J. P., Su, C.-H., and Takbashi, A.: A CMIP6-based multi-model downscaling ensemble to underpin climate change services in Australia, *Climate Services*, 30, 100368, <https://doi.org/10.1016/j.cliser.2023.100368>, 2023.
- Haylock, M. and McBride, J.: Spatial coherence and predictability of Indonesian wet season rainfall, *Journal of Climate*, 14, 3882–3887, [https://doi.org/10.1175/1520-0442\(2001\)014<3882:SCAPOI>2.0.CO;2](https://doi.org/10.1175/1520-0442(2001)014<3882:SCAPOI>2.0.CO;2), 2001.



- 805 Held, I. M., Guo, H., Adcroft, A., Dunne, J. P., Horowitz, L. W., Krasting, J., Shevliakova, E., Winton, M., Zhao, M., Bushuk, M., Wittenberg, A. T., Wyman, B., Xiang, B., Zhang, R., Anderson, W., Balaji, V., Donner, L., Dunne, K., Durachta, J., Gauthier, P. P. G., Ginoux, P., Golaz, J. C., Griffies, S. M., Hallberg, R., Harris, L., Harrison, M., Hurlin, W., John, J., Lin, P., Lin, S. J., Malyshev, S., Menzel, R., Milly, P. C. D., Ming, Y., Naik, V., Paynter, D., Paulot, F., Ramaswamy, V., Reichl, B., Robinson, T., Rosati, A., Seman, C., Silvers, L. G., Underwood, S., and Zadeh, N.: Structure and Performance of GFDL's  
810 CM4.0 Climate Model, *Journal of Advances in Modeling Earth Systems*, 11, 3691-3727, <https://doi.org/10.1029/2019MS001829>, 2019.
- Hersbach, H., Bell, B., Berrisford, P., Hirahara, S., Horányi, A., Muñoz-Sabater, J., Nicolas, J., Peubey, C., Radu, R., Schepers, D., Simmons, A., Soci, C., Abdalla, S., Abellan, X., Balsamo, G., Bechtold, P., Biavati, G., Bidlot, J., Bonavita, M., De Chiara, G., Dahlgren, P., Dee, D., Diamantakis, M., Dragani, R., Flemming, J., Forbes, R., Fuentes, M., Geer, A., Haimberger, L.,  
815 Healy, S., Hogan, R. J., Hólm, E., Janisková, M., Keeley, S., Laloyaux, P., Lopez, P., Lupu, C., Radnoti, G., de Rosnay, P., Rozum, I., Vamborg, F., Villaume, S., and Thépaut, J.-N.: The ERA5 global reanalysis, *Quarterly Journal of the Royal Meteorological Society*, 146, 1999-2049, <https://doi.org/10.1002/qj.3803>, 2020.
- Huang, B., Liu, C., Banzon, V., Freeman, E., Graham, G., Hankins, B., Smith, T., and Zhang, H.-M.: Improvements of the Daily Optimum Interpolation Sea Surface Temperature (DOISST) Version 2.1, *Journal of Climate*, 34, 2923-2939,  
820 <https://doi.org/10.1175/JCLI-D-20-0166.1>, 2021.
- Huang, B., Thorne, P. W., Banzon, V. F., Boyer, T., Chepurin, G., Lawrimore, J. H., Menne, M. J., Smith, T. M., Vose, R. S., and Zhang, H.-M.: Extended Reconstructed Sea Surface Temperature, Version 5 (ERSSTv5): Upgrades, Validations, and Intercomparisons, *Journal of Climate*, 30, 8179-8205, <https://doi.org/10.1175/JCLI-D-16-0836.1>, 2017.
- Ignacio-Reardon, S. and Luo, J.-j.: Evaluation of the Performance of CMIP6 Climate Models in Simulating Rainfall over the Philippines, *Atmosphere*, 14, 1459, 10.3390/atmos14091459, 2023.
- IPCC: Summary for Policymakers, in: *Climate Change 2022 - Mitigation of Climate Change: Working Group III Contribution to the Sixth Assessment Report of the Intergovernmental Panel on Climate Change*, edited by: Change, I. P. o. C., Cambridge University Press, Cambridge, UK and New York, NY, USA, 1-2, 10.1017/9781009157926.001., 2022.
- IPCC: Summary for Policymakers in: *Climate Change 2023: Synthesis Report*, edited by: Contribution of Working Groups I, I. a. I. t. S. A. R. o. t. I. P. o. C. C. C. W. T., H. Lee and J. Romero (eds.)), IPCC, Geneva, Switzerland, 1-34,  
830 0.59327/IPCC/AR6-9789291691647.001, 2023.
- Isphording, R. N., Alexander, L. V., Bador, M., Green, D., Evans, J. P., and Wales, S.: A Standardized Benchmarking Framework to Assess Downscaled Precipitation Simulations, *Journal of Climate*, 37, 1089-1110, <https://doi.org/10.1175/JCLI-D-23-0317.1>, 2024.
- 835 Jacob, D., Teichmann, C., Sobolowski, S., Katragkou, E., Anders, I., Belda, M., Benestad, R., Boberg, F., Buonomo, E., Cardoso, R. M., Casanueva, A., Christensen, O. B., Christensen, J. H., Coppola, E., De Cruz, L., Davin, E. L., Dobler, A., Domínguez, M., Fealy, R., Fernandez, J., Gaertner, M. A., García-Díez, M., Giorgi, F., Gobiet, A., Goergen, K., Gómez-Navarro, J. J., Alemán, J. J. G., Gutiérrez, C., Gutiérrez, J. M., Güttler, I., Haensler, A., Halenka, T., Jerez, S., Jiménez-Guerrero, P., Jones, R. G., Keuler, K., Kjellström, E., Knist, S., Kotlarski, S., Maraun, D., van Meijgaard, E., Mercogliano, P.,  
840 Montávez, J. P., Navarra, A., Nikulin, G., de Noblet-Ducoudré, N., Panitz, H.-J., Pfeifer, S., Piazza, M., Pichelli, E., Pietikäinen, J.-P., Prein, A. F., Preuschmann, S., Rechid, D., Rockel, B., Romera, R., Sánchez, E., Sieck, K., Soares, P. M. M., Somot, S., Srnec, L., Sørland, S. L., Termonia, P., Truhetz, H., Vautard, R., Warrach-Sagi, K., and Wulfmeyer, V.: Regional climate downscaling over Europe: perspectives from the EURO-CORDEX community, *Regional Environmental Change*, 20, 51, 10.1007/s10113-020-01606-9, 2020.



- 845 Jones, P. W.: First- and Second-Order Conservative Remapping Schemes for Grids in Spherical Coordinates, *Mon. Wea. Rev.*, 127, 2204–2210, [https://doi.org/10.1175/1520-0493\(1999\)127<2204-0493\(1999\)>2.0.CO;2](https://doi.org/10.1175/1520-0493(1999)127<2204-0493(1999)>2.0.CO;2), 1999.
- Juneng, L. and Tangang, F. T.: Evolution of ENSO-related rainfall anomalies in Southeast Asia region and its relationship with atmosphere–ocean variations in Indo-Pacific sector, *Climate Dynamics*, 25, 337–350, 2005.
- 850 Kamworapan, S., Bich Thao, P. T., Gheewala, S. H., Pimonsree, S., and Prueksakorn, K.: Evaluation of CMIP6 GCMs for simulations of temperature over Thailand and nearby areas in the early 21st century, *Heliyon*, 7, e08263, <https://doi.org/10.1016/j.heliyon.2021.e08263>, 2021.
- Kendall: Rank Correlation Coefficient, in, Springer New York, New York, NY, 278–281, [https://doi.org/10.1007/978-0-387-32833-1\\_211](https://doi.org/10.1007/978-0-387-32833-1_211), 1975.
- 855 Kim, Y.-H., Min, S.-K., Zhang, X., Sillmann, J., and Sandstad, M.: Evaluation of the CMIP6 multi-model ensemble for climate extreme indices, *Weather and Climate Extremes*, 29, 100269, <https://doi.org/10.1016/j.wace.2020.100269>, 2020.
- Knutti, R. and Sedláček, J.: Robustness and uncertainties in the new CMIP5 climate model projections, *Nature Climate Change*, 3, 369–373, [10.1038/nclimate1716](https://doi.org/10.1038/nclimate1716), 2013.
- Knutti, R., Furrer, R., Tebaldi, C., Cermak, J., and Meehl, G. A.: Challenges in Combining Projections from Multiple Climate Models, *Journal of Climate*, 23, 2739–2758, <https://doi.org/10.1175/2009jcli3361.1>, 2010.
- 860 Kucharski, F., Bracco, A., Barimalala, R., and Yoo, J. H.: Contribution of the east–west thermal heating contrast to the South Asian Monsoon and consequences for its variability, *Climate dynamics*, 37, 721–735, <https://doi.org/10.1007/s00382-010-0858-3>, 2011.
- Langenbrunner, B. and Neelin, J. D.: Analyzing ENSO Teleconnections in CMIP Models as a Measure of Model Fidelity in Simulating Precipitation, *Journal of Climate*, 26, 4431–4446, <https://doi.org/10.1175/JCLI-D-12-00542.1>, 2013.
- 865 Liu, Y. L., Alexander, L. V., Evans, J. P., and Thatcher, M.: Sensitivity of Australian rainfall to driving SST datasets in a variable-resolution global atmospheric model, <http://dx.doi.org/10.22541/essoar.170913616.69157157/v1>, 2024.
- Maraun, D. and Widmann, M.: Statistical downscaling and bias correction for climate research, Cambridge University Press, <https://doi.org/10.1017/9781107588783>, 2018.
- 870 Masson, D. and Knutti, R.: Spatial-Scale Dependence of Climate Model Performance in the CMIP3 Ensemble, *Journal of Climate*, 24, 2680–2692, <https://doi.org/10.1175/2011JCLI3513.1>, 2011.
- Mauritsen, T., Bader, J., Becker, T., Behrens, J., Bittner, M., Brokopf, R., Brovkin, V., Claussen, M., Crueger, T., Esch, M., Fast, I., Fiedler, S., Fläschner, D., Gayler, V., Giorgetta, M., Goll, D. S., Haak, H., Hagemann, S., Hedemann, C., Hohenegger, C., Ilyina, T., Jahns, T., Jimenez-de-la-Cuesta, D., Jungclaus, J., Kleinen, T., Kloster, S., Kracher, D., Kinne, S., Kleberg, D., Lasslop, G., Kornbluh, L., Marotzke, J., Matei, D., Meraner, K., Mikolajewicz, U., Modali, K., Möbis, B., Müller, W. A., Nabel, J. E. M. S., Nam, C. C. W., Notz, D., Nyawira, S.-S., Paulsen, H., Peters, K., Pincus, R., Pohlmann, H., Pongratz, J., Popp, M., Raddatz, T. J., Rast, S., Redler, R., Reick, C. H., Rohrschneider, T., Schemann, V., Schmidt, H., Schnur, R., Schulzweida, U., Six, K. D., Stein, L., Stemmler, I., Stevens, B., von Storch, J.-S., Tian, F., Voigt, A., Vrese, P., Wieners, K.-H., Wilkenskjaeld, S., Winkler, A., and Roeckner, E.: Developments in the MPI-M Earth System Model version 1.2 (MPI-ESM1.2) and Its Response to Increasing CO<sub>2</sub>, *Journal of Advances in Modeling Earth Systems*, 11, 998–1038, <https://doi.org/10.1029/2018MS001400>, 2019.
- 880



- McKenna, S., Santoso, A., Gupta, A. S., Taschetto, A. S., and Cai, W.: Indian Ocean Dipole in CMIP5 and CMIP6: characteristics, biases, and links to ENSO, *Scientific Reports*, 10, 11500, [10.1038/s41598-020-68268-9](https://doi.org/10.1038/s41598-020-68268-9), 2020.
- McSweeney, C. F., Jones, R. G., and Booth, B. B. B.: Selecting Ensemble Members to Provide Regional Climate Change Information, *Journal of Climate*, 25, 7100-7121, <https://doi.org/10.1175/JCLI-D-11-00526.1>, 2012.
- 885 McSweeney, C. F., Jones, R. G., Lee, R. W., and Rowell, D. P.: Selecting CMIP5 GCMs for downscaling over multiple regions, *Climate Dynamics*, 44, 3237-3260, <https://doi.org/10.1007/s00382-014-2418-8>, 2015.
- Meehl, G. A., Boer, G. J., Covey, C., Latif, M., and Stouffer, R. J.: The Coupled Model Intercomparison Project (CMIP), *Bulletin of the American Meteorological Society*, 81, 313-318, [https://doi.org/10.1175/1520-0477\(2000\)081<0313:Tcmipc>2.3.Co;2](https://doi.org/10.1175/1520-0477(2000)081<0313:Tcmipc>2.3.Co;2), 2000.
- 890 Meyers, G., McIntosh, P., Pigot, L., and Pook, M.: The Years of El Niño, La Niña, and Interactions with the Tropical Indian Ocean, *Journal of Climate*, 20, 2872-2880, <https://doi.org/10.1175/JCLI4152.1>, 2007.
- Mote, P., Brekke, L., Duffy, P. B., and Maurer, E.: Guidelines for constructing climate scenarios, *Eos, Transactions American Geophysical Union*, 92, 257-258, <https://doi.org/10.1029/2011EO310001>, 2011.
- Nearing, G. S., Ruddell, B. L., Clark, M. P., Nijssen, B., and Peters-Lidard, C.: Benchmarking and Process Diagnostics of Land Models, *Journal of Hydrometeorology*, 19, 1835-1852, <https://doi.org/10.1175/JHM-D-17-0209.1>, 2018.
- Nguyen, P.-L., Bador, M., Alexander, L. V., and Lane, T. P.: Selecting regional climate models based on their skill could give more credible precipitation projections over the complex Southeast Asia region, *Climate Dynamics*, 61, 3431-3452, [10.1007/s00382-023-06751-5](https://doi.org/10.1007/s00382-023-06751-5), 2023.
- 900 Nguyen, P.-L., Bador, M., Alexander, L. V., Lane, T. P., and Funk, C. C.: On the Robustness of Annual Daily Precipitation Maxima Estimates Over Monsoon Asia, *Frontiers in Climate*, 2, <https://doi.org/10.3389/fclim.2020.578785>, 2020.
- Nguyen, P.-L., Bador, M., Alexander, L. V., Lane, T. P., and Ngo-Duc, T.: More intense daily precipitation in CORDEX-SEA regional climate models than their forcing global climate models over Southeast Asia, *International Journal of Climatology*, n/a, <https://doi.org/10.1002/joc.7619>, 2022.
- 905 Nguyen-Duy, T., Ngo-Duc, T., and Desmet, Q.: Performance evaluation and ranking of CMIP6 global climate models over Vietnam, *Journal of Water and Climate Change*, 14, 1831-1846, [10.2166/wcc.2023.454](https://doi.org/10.2166/wcc.2023.454), 2023.
- Ossó, A., Craig, P., and Allan, R. P.: An assessment of CMIP6 climate signals and biases in temperature, precipitation and soil moisture over Europe, *International Journal of Climatology*, 43, 5698-5719, <https://doi.org/10.1002/joc.8169>, 2023.
- Overland, J. E., Wang, M., Bond, N. A., Walsh, J. E., Kattsov, V. M., and Chapman, W. L.: Considerations in the Selection of Global Climate Models for Regional Climate Projections: The Arctic as a Case Study, *Journal of Climate*, 24, 1583-1597, <https://doi.org/10.1175/2010JCLI3462.1>, 2011.
- 910 Palmer, T. E., McSweeney, C. F., Booth, B. B. B., Priestley, M. D. K., Davini, P., Brunner, L., Borchert, L., and Menary, M. B.: Performance-based sub-selection of CMIP6 models for impact assessments in Europe, *Earth Syst. Dynam.*, 14, 457-483, [10.5194/esd-14-457-2023](https://doi.org/10.5194/esd-14-457-2023), 2023.
- 915 Park, S., Shin, J., Kim, S., Oh, E., and Kim, Y.: Global Climate Simulated by the Seoul National University Atmosphere Model Version 0 with a Unified Convection Scheme (SAM0-UNICON), *Journal of Climate*, 32, 2917-2949, <https://doi.org/10.1175/JCLI-D-18-0796.1>, 2019.





- Perry, S. J., McGregor, S., Sen Gupta, A., England, M. H., and Maher, N.: Projected late 21st century changes to the regional impacts of the El Niño-Southern Oscillation, *Climate Dynamics*, 54, 395-412, [10.1007/s00382-019-05006-6](https://doi.org/10.1007/s00382-019-05006-6), 2020.
- 920 Pimonsree, S., Kamworapan, S., Gheewala, S. H., Thongbhakdi, A., and Prueksakorn, K.: Evaluation of CMIP6 GCMs performance to simulate precipitation over Southeast Asia, *Atmospheric Research*, 282, 106522, <https://doi.org/10.1016/j.atmosres.2022.106522>, 2023.
- Planton, Y. Y., Guilyardi, E., Wittenberg, A. T., Lee, J., Gleckler, P. J., Bayr, T., McGregor, S., McPhaden, M. J., Power, S., Roehrig, R., Vialard, J., and Voltaire, A.: Evaluating Climate Models with the CLIVAR 2020 ENSO Metrics Package, *Bulletin of the American Meteorological Society*, 102, E193-E217, <https://doi.org/10.1175/BAMS-D-19-0337.1>, 2021.
- 925 Power, S. B. and Delage, F. P. D.: El Niño–Southern Oscillation and Associated Climatic Conditions around the World during the Latter Half of the Twenty-First Century, *Journal of Climate*, 31, 6189-6207, <https://doi.org/10.1175/JCLI-D-18-0138.1>, 2018.
- Qian, J.-H., Robertson, A. W., and Moron, V.: Diurnal cycle in different weather regimes and rainfall variability over Borneo associated with ENSO, *Journal of Climate*, 26, 1772-1790, <https://doi.org/10.1175/JCLI-D-12-00178.1>, 2013.
- 930 Rayner, N. A., Parker, D. E., Horton, E. B., Folland, C. K., Alexander, L. V., Rowell, D. P., Kent, E. C., and Kaplan, A.: Global analyses of sea surface temperature, sea ice, and night marine air temperature since the late nineteenth century, *Journal of Geophysical Research: Atmospheres*, 108, <https://doi.org/10.1029/2002JD002670>, 2003.
- Ridder, N. N., Pitman, A. J., and Ukkola, A. M.: Do CMIP6 Climate Models Simulate Global or Regional Compound Events Skillfully?, *Geophysical Research Letters*, 48, e2020GL091152, <https://doi.org/10.1029/2020GL091152>, 2021.
- 935 Rousseeuw, P. J.: Silhouettes: A graphical aid to the interpretation and validation of cluster analysis, *Journal of Computational and Applied Mathematics*, 20, 53-65, [https://doi.org/10.1016/0377-0427\(87\)90125-7](https://doi.org/10.1016/0377-0427(87)90125-7), 1987.
- Saji, N. H., Goswami, B. N., Vinayachandran, P. N., and Yamagata, T.: A dipole mode in the tropical Indian Ocean, *Nature*, 401, 360-363, [10.1038/43854](https://doi.org/10.1038/43854), 1999.
- 940 Schamm, K., Ziese, M., Becker, A., Finger, P., Meyer-Christoffer, A., Schneider, U., Schröder, M., and Stender, P.: Global gridded precipitation over land: a description of the new GPCP First Guess Daily product, *Earth Syst. Sci. Data*, 6, 49-60, <https://doi.org/10.5194/essd-6-49-2014>, 2014.
- Seland, Ø., Bentsen, M., Olivie, D., Toniazzo, T., Gjermundsen, A., Graff, L. S., Debernard, J. B., Gupta, A. K., He, Y. C., Kirkevåg, A., Schwinger, J., Tjiputra, J., Aas, K. S., Bethke, I., Fan, Y., Griesfeller, J., Grini, A., Guo, C., Ilicak, M., Karset, I. H. H., Landgren, O., Liakka, J., Moseid, K. O., Nummelin, A., Spensberger, C., Tang, H., Zhang, Z., Heinze, C., Iversen, T., and Schulz, M.: Overview of the Norwegian Earth System Model (NorESM2) and key climate response of CMIP6 DECK, historical, and scenario simulations, *Geosci. Model Dev.*, 13, 6165-6200, [10.5194/gmd-13-6165-2020](https://doi.org/10.5194/gmd-13-6165-2020), 2020.
- 945 Sellar, A. A., Jones, C. G., Mulcahy, J. P., Tang, Y., Yool, A., Wiltshire, A., O'Connor, F. M., Stringer, M., Hill, R., Palmieri, J., Woodward, S., de Mora, L., Kuhlbrodt, T., Rumbold, S. T., Kelley, D. I., Ellis, R., Johnson, C. E., Walton, J., Abraham, N. L., Andrews, M. B., Andrews, T., Archibald, A. T., Berthou, S., Burke, E., Blockley, E., Carslaw, K., Dalvi, M., Edwards, J., Folberth, G. A., Gedney, N., Griffiths, P. T., Harper, A. B., Hendry, M. A., Hewitt, A. J., Johnson, B., Jones, A., Jones, C. D., Keeble, J., Liddicoat, S., Morgenstern, O., Parker, R. J., Predoi, V., Robertson, E., Sahaan, A., Smith, R. S., Swaminathan, R., Woodhouse, M. T., Zeng, G., and Zerroukat, M.: UKESM1: Description and Evaluation of the U.K. Earth System Model, *Journal of Advances in Modeling Earth Systems*, 11, 4513-4558, <https://doi.org/10.1029/2019MS001739>, 2019.



- Shukla, R. P., Tripathi, K. C., Pandey, A. C., and Das, I.: Prediction of Indian summer monsoon rainfall using Niño indices: a neural network approach, *Atmospheric Research*, 102, 99-109, 2011.
- Sobolowski, S., Somot, S., Fernandez, J., Evin, G., Maraun, D., Kotlarski, S., Jury, M., Benestad, R. E., Teichmann, C., Christensen, O. B., Bülow, K., Buonomo, E., Katragkou, E., Steger, C., Sørland, S., Nikulin, G., McSweeney, C., Dobler, A., Palmer, T., Wilcke, R., Boé, J., Brunner, L., Ribes, A., Qasmi, S., Nabat, P., Sevault, F., Oudar, T., and Brands, S.: EURO-CORDEX CMIP6 GCM Selection & Ensemble Design: Best Practices and Recommendations, Zenodo, <https://doi.org/10.5281/zenodo.7673400>, 2023.
- Supari, S., Tangang, F., Salimun, E., Aldrian, E., Sopaheluwakan, A., and Juneng, L.: ENSO modulation of seasonal rainfall and extremes in Indonesia, *Climate Dynamics*, 51, 10.1007/s00382-017-4028-8, 2018.
- Tangang, F., Chung, J. X., Juneng, L., Supari, Salimun, E., Ngai, S. T., Jamaluddin, A. F., Mohd, M. S. F., Cruz, F., Narisma, G., Santisirisomboon, J., Ngo-Duc, T., Van Tan, P., Singhruck, P., Gunawan, D., Aldrian, E., Sopaheluwakan, A., Grigory, N., Remedio, A. R. C., Sein, D. V., Hein-Griggs, D., McGregor, J. L., Yang, H., Sasaki, H., and Kumar, P.: Projected future changes in rainfall in Southeast Asia based on CORDEX-SEA multi-model simulations, *Climate Dynamics*, 55, 1247-1267, <https://doi.org/10.1007/s00382-020-05322-2>, 2020.
- Tangang, F. T., Juneng, L., Salimun, E., Sei, K., and Halimatun, M.: Climate change and variability over Malaysia: gaps in science and research information, *Sains Malaysiana*, 41, 1355-1366, 2012.
- Taschetto, A. S., Gupta, A. S., Jourdain, N. C., Santoso, A., Ummerhofer, C. C., and England, M. H.: Cold Tongue and Warm Pool ENSO Events in CMIP5: Mean State and Future Projections, *Journal of Climate*, 27, 2861-2885, <https://doi.org/10.1175/JCLI-D-13-00437.1>, 2014.
- Tatebe, H., Ogura, T., Nitta, T., Komuro, Y., Ogochi, K., Takemura, T., Sudo, K., Sekiguchi, M., Abe, M., Saito, F., Chikira, M., Watanabe, S., Mori, M., Hirota, N., Kawatani, Y., Mochizuki, T., Yoshimura, K., Takata, K., O'Ishi, R., Yamazaki, D., Suzuki, T., Kurogi, M., Kataoka, T., Watanabe, M., and Kimoto, M.: Description and basic evaluation of simulated mean state, internal variability, and climate sensitivity in MIROC6, *Geosci. Model Dev.*, 12, 2727-2765, 10.5194/gmd-12-2727-2019, 2019.
- Trenberth, K. E. and Hoar, T. J.: El Niño and climate change, *Geophysical Research Letters*, 24, 3057-3060, <https://doi.org/10.1029/97GL03092>, 1997.
- Vincent, C. L. and Lane, T. P.: Evolution of the diurnal precipitation cycle with the passage of a Madden-Julian oscillation event through the Maritime Continent, *Monthly Weather Review*, 144, 1983-2005, <https://doi.org/10.1175/MWR-D-15-0326.1>, 2016.
- Voltaire, A., Saint-Martin, D., Sénési, S., Decharme, B., Alias, A., Chevallier, M., Colin, J., Guérémy, J.-F., Michou, M., Moine, M.-P., Nabat, P., Roehrig, R., Salas y Méria, D., Sférian, R., Valcke, S., Beau, I., Belamari, S., Berthet, S., Cassou, C., Cattiaux, J., Deshayes, J., Douville, H., Ethé, C., Franchistéguy, L., Geoffroy, O., Lévy, C., Madec, G., Meurdesoif, Y., Msadek, R., Ribes, A., Sanchez-Gomez, E., Terray, L., and Waldman, R.: Evaluation of CMIP6 DECK Experiments With CNRM-CM6-1, *Journal of Advances in Modeling Earth Systems*, 11, 2177-2213, <https://doi.org/10.1029/2019MS001683>, 2019.
- Volodin, E. M., Mortikov, E. V., Kostykin, S. V., Galin, V. Y., Lykosov, V. N., Gritsun, A. S., Diansky, N. A., Gusev, A. V., and Yakovlev, N. G.: Simulation of modern climate with the new version of the INM RAS climate model, *Izvestiya, Atmospheric and Oceanic Physics*, 53, 142-155, 10.1134/S0001433817020128, 2017.



- Wang, B., Luo, X., and Liu, J.: How Robust is the Asian Precipitation–ENSO Relationship during the Industrial Warming Period (1901–2017)?, *Journal of Climate*, 33, 2779–2792, <https://doi.org/10.1175/JCLI-D-19-0630.1>, 2020.
- 995 Wang, Y.-C., Hsu, H.-H., Chen, C.-A., Tseng, W.-L., Hsu, P.-C., Lin, C.-W., Chen, Y.-L., Jiang, L.-C., Lee, Y.-C., Liang, H.-C., Chang, W.-M., Lee, W.-L., and Shiu, C.-J.: Performance of the Taiwan Earth System Model in Simulating Climate Variability Compared With Observations and CMIP6 Model Simulations, *Journal of Advances in Modeling Earth Systems*, 13, e2020MS002353, <https://doi.org/10.1029/2020MS002353>, 2021a.
- Wang, Z., Zhan, C., Ning, L., and Guo, H.: Evaluation of global terrestrial evapotranspiration in CMIP6 models, *Theoretical and Applied Climatology*, 143, 521–531, <https://doi.org/10.1007/s00704-020-03437-4>, 2021b.
- 1000 Wu, T., Lu, Y., Fang, Y., Xin, X., Li, L., Li, W., Jie, W., Zhang, J., Liu, Y., Zhang, L., Zhang, F., Zhang, Y., Wu, F., Li, J., Chu, M., Wang, Z., Shi, X., Liu, X., Wei, M., Huang, A., Zhang, Y., and Liu, X.: The Beijing Climate Center Climate System Model (BCC-CSM): the main progress from CMIP5 to CMIP6, *Geosci. Model Dev.*, 12, 1573–1600, 10.5194/gmd-12-1573-2019, 2019.
- 1005 Xu, J., Koldunov, N. V., Xu, M., Zhu, X., Fraedrich, K., Jiang, X., Zhu, S., and Zhi, X.: Impacts of Indian Ocean Dipole–Like SST on Rice Yield Anomalies in Jiangsu Province, *Frontiers in Earth Science*, 8, 690, <https://doi.org/10.3389/feart.2020.568365>, 2021.
- Yatagai, A., Kamiguchi, K., Arakawa, O., Hamada, A., Yasutomi, N., and Kitoh, A.: APHRODITE: Constructing a Long-Term Daily Gridded Precipitation Dataset for Asia Based on a Dense Network of Rain Gauges, *Bulletin of the American Meteorological Society*, 93, 1401–1415, <https://doi.org/10.1175/BAMS-D-11-00122.1>, 2012.
- 1010 Yukimoto, S., Kawai, H., Koshiro, T., Oshima, N., Yoshida, K., Urakawa, S., Tsujino, H., Deushi, M., Tanaka, T., Hosaka, M., Yabu, S., Yoshimura, H., Shindo, E., Mizuta, R., Obata, A., Adachi, Y., and Ishii, M.: The Meteorological Research Institute Earth System Model Version 2.0, MRI-ESM2.0: Description and Basic Evaluation of the Physical Component, *Journal of the Meteorological Society of Japan. Ser. II*, 97, 931–965, 10.2151/jmsj.2019-051, 2019.
- 1015 Zheng, X., Li, Q., Zhou, T., Tang, Q., Van Roekel, L. P., Golaz, J. C., Wang, H., and Cameron-Smith, P.: Description of historical and future projection simulations by the global coupled E3SMv1.0 model as used in CMIP6, *Geosci. Model Dev.*, 15, 3941–3967, 10.5194/gmd-15-3941-2022, 2022.
- Ziehn, T., Chamberlain, M. A., Law, R. M., Lenton, A., Bodman, R. W., Dix, M., Stevens, L., Wang, Y.-P., and Srbinovsky, J.: The Australian Earth System Model: ACCESS-ESM1.5, *Journal of Southern Hemisphere Earth Systems Science*, 70, 193–214, <https://doi.org/10.1071/ES19035>, 2020.
- 1020